CONTEXT-AWARE CONGESTION CONTROL FOR PEDESTRIAN SAFETY COMMUNICATION

by

ALI ROSTAMI

A dissertation submitted to the

School of Graduate Studies

Rutgers, The State University of New Jersey

in partial fulfillment of the requirements

for the degree of

Doctor of Philosophy

Graduate Program in Electrical and Computer Engineering

Written under the direction of

Marco Gruteser

and approved by

_____

_____

_____

_____

New Brunswick, New Jersey

January, 2020

ABSTRACT OF THE DISSERTATION

Context-Aware Congestion Control for Pedestrian Safety Communication

by Ali Rostami

Dissertation Director:

Marco Gruteser

Pedestrian-to-Everything (P2X) communication has numerous advantages from improving traffic light cycle schedules to increase pedestrian safety. Challenges, such as handling the lack of positioning accuracy in urban canyons, limited battery power, and wireless channel resources, still need to be addressed before mass deployment of these systems. The goal of this research is to introduce a distributed channel congestion control algorithm for Personal Safety Messages (PSMs) that can converge in heterogeneous application environments with different message rates. Different message rates arise, for example, with contextual transmission policies (CTP) that activate different applications based on situational context, such as the estimated positioning accuracy. Energy consumption is another challenge when smartphones are used to enhance pedestrian safety. Therefore, to minimize channel sensing energy usage, we further propose a novel collaborative channel load measurement mechanism, as opposed to more conventional approaches employed in Vehicle-to-Vehicle (V2V) communication.

To properly tackle the problem, an accurate network simulator is important to understand how P2X communication performs for different algorithms and approaches. More specifically, the aforementioned simulator needs to accurately model the following components: (*i*) Channel propagation with co-channel interference in 5.9 GHz band with 10 MHz bandwidth, (*ii*) realistic positioning model as part of the system, i.e.

smartphones, that P2X transmissions take place, and (*iii*) realistic dense mobility scenarios. Therefore, we start with modeling and calibrating channel propagation for Dedicated Short-Range Communications (DSRC) in the 5.9 GHz DSRC band in an intersection environment. Then, we evaluate channel performance under an idealized positioning accuracy for a realistic mobility scenario. Then, the steps taken to investigate different approaches to reduce unnecessary P2X transmissions are shown. Finally, we develop a multi-rate congestion controller that improves smartphones battery consumption and information age. Extensive simulations show that when the proposed algorithms are used, information age for P2X safety applications is improved, which potentially increases pedestrian safety, and the energy consumption is significantly reduced.

Acknowledgements

I would like to thank my advisor and my mentor, Professor Marco Gruteser. I have learned so much from you, and words cannot describe my gratitude to you. Your profound belief in my abilities had always kept me going. I deeply feel fortunate for having you as my advisor.

I would also like to thank Prof. Roy Yates, Prof. Richard Martin, Dr. John Kenney, and Prof. Dipankar Raychaudhuri, my proposal and dissertation committee members, for the insightful discussions and their constructive comments. I also wish to express my gratitude to my collaborators at CAMP—especially Steve VanSickle.

My special appreciation to my teammate and my friend, Dr. Bin Cheng, for always being there for me. Your sharp mind was the key to resolve many of our mutual problems during all the years we worked together. I would like to thank the WINLAB engineering team and staff for their support. I was very lucky to be surrounded by a sharp, professional, and supportive team.

I wish to acknowledge the support and great love of my family. You made me who I am today. Love you to the moon and back.

Last but not least; Dragoslav, Jake, Jenny, Parishad, Mohsen R., Mila, Kian, Aydin, Danial, Delara, Behnam, Sam, Shahab, Shirin, Tannaz, Ardeshir, Rahil, Mina, Amir, Sonia, Navid, Davood, Mahsa, Amirali, Elham, Hooman, Maryam, Farnood, Farzaneh, Reza, Farhad, Mozhgan, Zahra, Mehdi, Arian, Mahtab, Shadi, Nora, Yasi, Ines, Mohammad H., Mohsen Gh., and Siamak: Thank you for being my second family. You have been by my side in many of my ups and downs in my new home. I will always keep our memories in my heart.

Dedication

To the passengers of PS752 and their families.

Table of Contents

List of Tables

List of Figures

Chapter 1

Introduction

1.1 Motivation

Vulnerable Road Users (VRUs) are traffic participants who are at higher risk for serious injury or death in case of an accident than car occupants. Examples are pedestrians, pedalcyclists, and road workers. Among them, pedestrians represent 84% of the 6421 total United States VRU fatalities during 2015 [1]. Research by the National Highway Traffic Safety Administration (NHTSA) also shows a 10% increase in the VRU fatality rate from 2014 to 2015 [2]. These trends and the significant number of accidents motivates the quest for technology solutions to improve VRU safety.

Pedestrians account for a sizable share of traffic fatalities. Even in the United States, where walking is a less common mode of transportation than in other parts of the world, 4,910 pedestrians were killed and more than 65,000 injured in 2014 only [2]. The number pedestrian fatality grows over 12% in 2015 and another 9% in 2016 [3]. This represents about 15% of traffic fatalities. According to World Health Organization (WHO), the share rises to one third in less developed countries [4]. This motivated the research community to develop technologies to increase pedestrian safety.

Previous work has largely considered stand-alone approaches using vehicle sensors, and more recently smartphones, to enhance safety for VRU. Automakers have developed camera, RADAR, infrared, and LIDAR based sensors to detect pedestrians in a vehicle's path [5]. Vehicles can use this information to alert drivers or to automatically avoid or reduce the severity of the crash. Recent more exploratory work has investigated whether a smartphone camera can be used while talking on the phone to detect approaching vehicles and warn the pedestrian [6]. All these technologies require line-of-sight (LOS) between the pedestrian and the vehicle, however. They are inherently less effective

when a pedestrian emerges between parked vehicles or in other scenarios where the time to react is too short once line-of-sight exists.

To create earlier awareness of potentially dangerous situations, even without line-of-sight, researchers have designed collaborative approaches that rely on wireless communications. An example of this category is an RFID-based proximity detection technique that identifies pedestrians at the intersections via Road-Side Units (RSU) and forwards the information to the approaching vehicles [7].

1.2 DSRC-Based Connected Vehicles Technology

There are numerous advantages for smartphones from vulnerable road users to communicate with vehicles and infrastructure in a smart city. Some of these are demonstrated in the Connected Vehicles Pilot Deployment (CVPD) programs launched by the United States Department of Transportation (USDOT) [8]. These programs are focused on safety applications that aim to reduce—or even to eliminate—accident-related deaths, injuries and damages. Two of the three programs include pedestrian smartphones that communicate with infrastructure or vehicles. The New York City CVPD program, for example, pilots a DSRC-assisted application for pedestrians, wherein smartphones communicate with road-side infrastructure to assist visually impaired pedestrian with providing intersection geometry and traffic light phase information in verbal form [9].

One line of work to improve VRU safety explores the use of smartphones or other personal devices to send Personal Safety Messages (PSM) which inform surrounding vehicles of the presence and location of VRUs. For example, Tahmasbi et al. [10] developed a Dedicated Short Range Communications-based collision detection system wherein a vehicle and a smartphone can directly communicate. To ensure that approaching vehicles have the most recent information about a VRU, including its location, speed and heading, such PSM messages must be sent repeatedly. This raises questions about the performance of communication-based pedestrian safety technologies—and a possibility of needing a channel congestion controller—in crowded areas.

1.3 Congestion Control in Connected Vehicles Systems

A technical challenge, as reported in Chapter 4, is high channel usage which is caused by an overwhelming amount of VRU devices transmitting PSMs through a channel of limited bandwidth. The overloaded channel results in significant transmission errors for PSMs and may degrade the networking performance for all other types of messages sharing the same wireless medium.

For vehicle-to-vehicle (V2V) safety messages, prior work has addressed channel congestion through different congestion control algorithms. It focuses on adjusting the message rate of each vehicle based on vehicle dynamics or parameters such as Channel Busy Percentage (CBP) measurements (e.g.,[11, 12]). However, it is nontrivial to address this scalability challenge for PSM transmission by simply applying congestion control algorithms from the V2V cooperative safety community which has extensively investigated the scalabiilty issue for Basic Safety Message (BSM) transmissions. The primary reasons are threefold:

First, the density of pedestrians can be higher than that of vehicles, which lead to even more congested channels. A city plaza such as Times Square in Manhattan, New York City, is an example of such environments that many smartphones can operate on the same channel.

Second, a VRU device usually has a limited capacity of battery, making it undesirable to transmit PSMs at a high message rate all the time, in other words, regardless if a VRU is exposed to a possibility of a traffic accident. This is different with V2V communications that are not subject to energy constraint and could transmit BSMs independent of the presence of a vehicle crash threat. As a result, the developed V2V congestion control algorithms, which allow vehicles to always transmit BSMs at a large rate when the channel is not deemed congested, do not directly suit management of PSM transmission.

Third, VRU experiences a set of safety contexts for which the V2V congestion control algorithms may not have an appropriate wireless resource allocation when channel is overused. More specifically, popular V2V congestion control solutions emphasize

fairness when allocating wireless resource to vehicles [11, 12]. This leads vehicles with equal chances to transmit BSMs since it is both important to hear others and to be heard on the road. For PSM transmissions, however, VRUs have no interests in hearing each other for road safety purpose. They instead need to be known by vehicles. Their vulnerability with respect to oncoming vehicles, as compared to fairness, could be a better metric based on which wireless resources allocation can be determined, particularly since the risk of collision with a vehicle is very unevenly distributed for pedestrians (located in-street vs sidewalk, for example).

1.4 Thesis Objectives

While the above activities help advance the P2X communication technology, P2X is still at an early stage. Several technical challenges remain to be addressed before such technology can be deployed. For example, the DSRC community aims for lane-level accuracy in its messages but the localization technology required to provide at least lane-level accuracy [13] is not available to today's portable devices (e.g. smartphones), which will likely be the main type of equipment transmitting PSMs.

In particular, the objective of this thesis is to design a multi-rate channel controller to control congestion on a 10 MHz channel for PSM transmissions in a heterogeneous application environment. The list of contributions of the thesis are as follow:

1. **Modeling 5.9 GHz signal propagation at a reference intersection.** The channel behavior is significantly defined by the environment. Intersections are an especial type of environment that enables communications between transceivers, where buildings obstruct line-of-sight. The provided calibrated model considers the impact of the buildings on signal propagation on 5.9 GHz band.

2. **Performance and Channel Load Evaluation for Pedestrian Transmissions.** The very first step towards the main thesis objective is to understanding P2X communications. The contributions ar providing a comprehensive simulation scenario of Manhattan, and evaluating P2X communication with both idealized and realistic positioning systems.

3. **Multi-rate Congestion Controller for Pedestrian Communication.** Time- and location-dependent characteristics of PSM application requirements makes it challenging to reuse solutions which are originally designed for V2V communication. A multi-rate channel controller can adjust message rate by considering varying application requirements and provide proportional fairness.

1.5 Thesis Organization

The thesis is organized as follows: After the introduction by the current chapter, Chapter 2 goes over the efforts towards modeling channel propagation in an intersection environment. The provided model is calibrated for a reference intersection in Los Angles, California, and it is used to design a simulator suited for P2X communication, which is introduced in Chapter 3. In addition, Chapter 3 discusses the other elements of the pedestrian communication simulator, such as a calibrated dense pedestrian mobility trace for a Manhattan scenario. This thesis, then, takes the initiatives on P2X communication in Chapter 4 by evaluating the scenario for pedestrian communication regarding the channel load and congestion level with an idealized positioning system assumption. Chapter 5 relaxes the assumption by proposing a heuristic for reducing pedestrian transmissions when the positioning system contains a realistic error. Chapter 6 offers a multi-rate congestion controller for pedestrian communication and shows the performance of the system in terms of Information Age (IA) when employing the proposed algorithm. The dissertation is concluded in Chapter 7.

Chapter 2

Modeling Propagation at 5.9 GHz for a Reference Intersection

Intersections are of particular interest for simulation due to their more complex nature in terms of wireless channel propagation. Buildings and other structures introduce Non-Line-of-Sight (NLOS)—or Obstructed Line-of-Sight (OLOS), as some studies refer to it—one of the complexities that demands for a customized model rather than the propagation models used for free-space communication. Intersections are also of particular interest for studying connected vehicles' applications as they are accident hotspots and create significant driving risks. In particular, the Manhattan scenario, which is developed for evaluating the proposed solutions in this thesis, contains a lot of intersections. Although, the test environment is not a perfect match, to our best knowledge, the dataset used to model and calibrate an intersection environment—presented in this chapter—is one of the largest available to the date.

2.1 Previous Models

Previous work in the literature emphasizes the importance of the accuracy of the channel model on protocol evaluations through simulation [14]. Some of the previous work focus on cellular vehicle-to-everything (C-V2X) communication [15], while this paper focuses on DSRC and modeling propagation in a 10 MHz narrow-band wireless channel in 5.9 GHz band.

Many vehicle-to-vehicle data collection campaigns have analyzed the impact of non-line-of-sight (NLOS), also referred to as Obstructed Line-of-Sight (OLOS), due to obstructing buildings [16, 17, 18, 19]. The common observation of these studies is that the propagation behavior of the channel significantly differs for line-of-sight (LOS) and

NLOS communication cases.

Obstructions of line-of-sight propagation can occur due to structures such as buildings or other vehicular traffic. Several lines of work focus on NLOS communication due to other vehicular traffic [20, 21], and they all show the significant impact of the ongoing vehicular traffic on channel propagation behavior.

Sommer et al. [22] propose a propagation loss model to calculate the attenuation for radio signals due to passing through walls of obstructing buildings. The model captures the fading caused by the buildings by deducting an average of 9.2 dB per exterior wall from the received signal strength. In addition, it approximates the impact of interior obstructions based on an attenuation coefficient that depend on the distance that the radio signal travels inside the building. This model is the default propagation loss model for communications at intersection scenarios in the Veins simulator [23]. The model, however, does not account for rapid wireless channel changes. Equation 2.1 represents the model as follows.

$$P_{rx} = P_{tx} + 10\log_{10}\left(\frac{G_{tx}G_{rx}\lambda^2}{16\pi^2 d^{\alpha}}\right) - \beta n - \gamma d_m \tag{2.1}$$

Where λ is wavelength, d is the distance between TX and RX, α is the path loss exponent, β is the coefficient of loss for n exterior walls, γ is the coefficient of the amount of loss per meter for the distance d_m that the signal travels withing the buildings. In our simulations, we used α=2.2, β=9.2 dB, and γ=0.32 dB/m as indicated in [22].

Mangel et al. [24] gather V2V radio data from eight different intersections in Munich and further analyzed them to understand the impact of the obstructing buildings on the wireless link in the 5.9 GHz band. The authors derived a propagation model that accounts for the road width, the distance of the transmitter from the wall, and the distance of the transmitter and receiver from the center of intersection. The data analysis by this study shows that 50% of the packets are lost at a distance between 40-160 m, depending on intersections. The authors derive a generalized propagation loss model for NLOS communications at intersections. Equation 2.2 represents the model as follows.

$$P_{rx} = P_{tx} - C - L_{su} - 10\log_{10}\left(\left(\frac{d_t^{E_T} 4\pi d_R}{(x_t w_r)^{E_S}\lambda}\right)^{E_L}\right) \tag{2.2}$$

Where C is a constant, L_{su} is a constant loss only for suburban areas, E_T is TX distance exponent, E_S is street exponent, E_L is loss exponent, and d_R is equal to d_r, i.e. the distance of RX to the intersection center, for distances less than 150 m, otherwise, it is equal to d_r^2. x_t represents the distance of TX to the building's wall, and w_r is the road width where RX is located. As indicated in [24], C=3.75, L_{su}=2.94, E_T=0.957, E_S=0.81, and E_L=2.69 are used for our simulation comparison in Section 2.5.

To the best of our knowledge, the above models do not account for the real vehicular traffic. In this paper we aim to address the factors with high impact on signal propagation. Our proposed hybrid model captures an average impact of both ongoing vehicular traffic and building shadowing by fitting parameters based on experiment data, as well as addressing sparse building structure at intersections in suburban area by geometrical components.

2.2 Data Collection Campaign

To understand the propagation characteristics at intersections we co-developed field experiments wherein 10 sedan cars equipped with DSRC radios drive through an intersection among regular vehicular traffic. In addition to the test fleet, a Command and Control Center (CnC) was deployed to help coordinate and monitor the vehicle trips in these experiments so that they meet at the intersection of interest while traveling in regular traffic.

2.2.1 Experiment Site

Figure 2.1 shows the selected intersection for the experiment. The data collection campaign was part of a larger effort for evaluating V2V congestion control algorithms in high vehicular traffic density scenarios. Therefore, the intersection of Westminster Blvd and Beach Blvd in Orange County, CA was chosen, an intersection with four and eight lanes (see Figure 2.1a and 2.3) and relatively busy traffic.

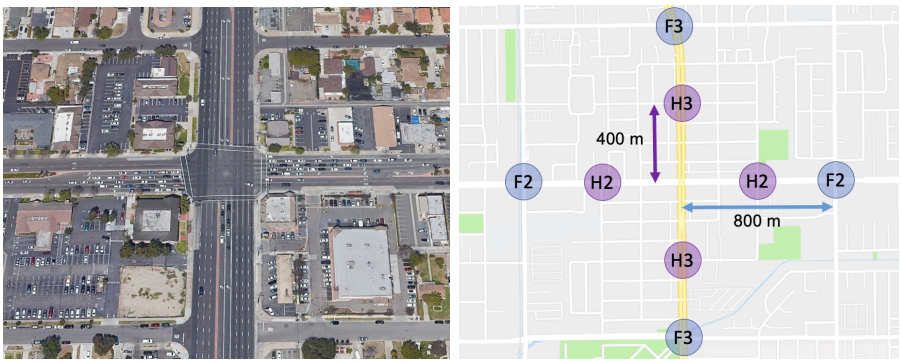

(a) (b)

Figure 2.1: (a) Bird's-eye view of the intersection, and (b) experiment scenarios and start/finish locations on the map.

2.2.2 Test Fleet

As for the test cars, 10 sedans were chosen through rental services with low profile antennas, no sun-roofs, and about the same height. Table 2.1 shows basic information about the test cars. The test cars were equipped with a DSRC On-Board Equipment (OBE) unit capable of transmitting and receiving standard Basic Safety Message (BSM) packets, a GPS receiver with 10 Hz sampling to feed location of the car into the BSM packets and vehicle logs. The vehicles were also equipped with walkie-talkie radios and phones on a conference call for coordinating start of test trips.

Table 2.1: Description of test cars

Brand & Model	**Height**
Volkswagen Passat (×3)	148.59 cm
Mitsubishi Lancer	148.08 cm
Nissan Altima	147.07 cm
Nissan Sentra	149.60 cm
Kia Optima (×3)	146.56 cm
Ford Fusion SE	147.57 cm

Test cars were also carrying an additional UHF transmitter to transmit their live location to the CnC. The operator at the CnC used the live location information illustrated on Google Earth to coordinate the start of each group of test cars to increase the chance that they would meet in the area of interest near the intersection. Note that once the start command was given, speed was influenced by other vehicular traffic.

The OBE consisted of a DSRC unit capable of transmitting and receiving BSM

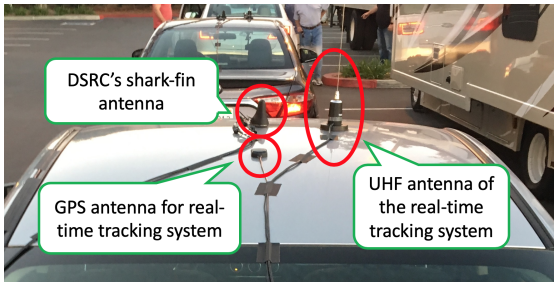

Figure 2.2: Antenna setup on the roof of one of the test cars.

packets. All packet transmissions and receptions, as well as any available GPS sample were logged to support the analysis.To increase the number of signal strength samples for analysis, the message transmission rate of the OBEs was configured to be 20 Hz and security payloads were disabled yielding smaller packets. Given ten vehicles and the smaller packet size, the chance that one vehicle would interfere with another was negligible.

Figure 2.2 illustrates one of the test cars with different antennas mounted on the roof. As seen, the DSRC and GPS (and a WiFi radio for remote configuration management), were connected to a shark-fin antenna that was mounted at the center of the roof. An additional UHF antenna for experiment coordination (vehicle position tracking) was mounted on the passenger-side roof edge, i.e. right side of the shark fin antenna. Overall, our characterization tests show good omnidirectinal signal propagation for DSRC signals.

2.2.3 Experiment Plan

The test fleet was divided into four groups of cars so that one group could cover every intersection leg in each experiment pass. The larger groups of three cars, (letters marked by number 3 in Figure 2.1b), were assigned to Beach Blvd because it has more lanes. Two major scenario were performed: 1) in the *Full-Block* scenario, marked by F in Figure 2.1b, all groups of test cars start one block away from the intersection (≈800 m away from the intersection center) and finish their experiment pass at the opposite F point; 2) in the *Half-Block* scenario, marked by letter H in Figure 2.1b, vehicles start ≈400 m away from the center of the intersection. Test cars pass the intersection until

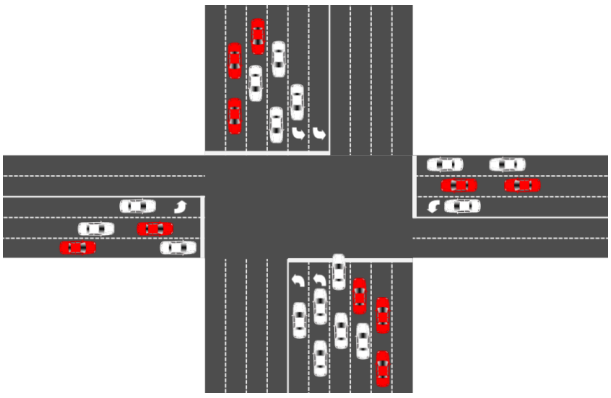

Figure 2.3: Example of an experiment pass where all the test cars (depicted in red) meet at the intersection.

arriving at the opposite H point.

2.3 Data Analysis

At the post-processing stage, the collected dataset is analyzed from different angles. We start with dividing the dataset based on the location of test cars for each log entry. Then, we study the differences between median RSS decaying behavior over transmitter-receiver (TX-RX) distance for different propagation conditions.

2.3.1 Model Intuition

Let us start with comparing the RSS of received packets under different propagation conditions. Figure 2.4 compares about half a million RSS samples for received BSMs where the pair of transceivers are located on intersecting roads, to more than 1.5 million RSS samples for BSM receptions where the pair are locate on the same road. We will refer to former as *Around-the-Corner* (ATC) propagation, and the latter as *Longitudinal* propagation for the rest of the paper. In both figures, the distribution of RSS (blue dots) is shown via different percentiles for 5 m Tx-Rx distance bins, shaded in different colors. As it can be seen, the pathloss is significantly higher for the ATC propagation in comparison with the Longitudinal propagation, showing ≈10 dB difference as the median RSS at 100 m.

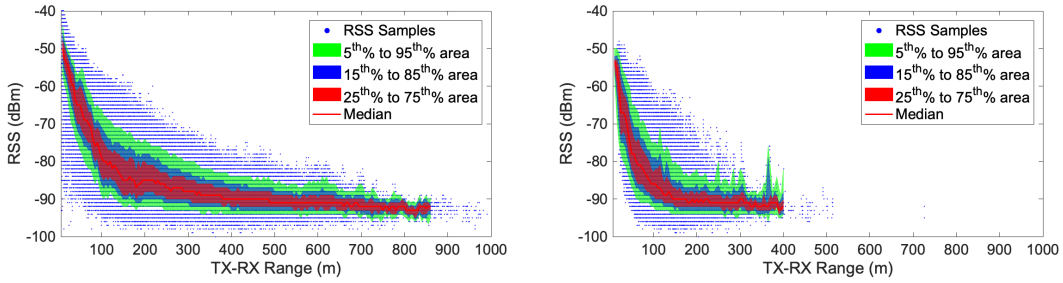

(a) (b)

Figure 2.4: RSS comparison for received BSMs in (a) Longitudinal, and (b) ATC propagation.

2.3.2 Impact of Buildings and Traffic

Building Structure. Unlike Longitudinal propagation, wherein the pathloss component is mainly a function of the TX-RX, in ATC propagation a signal might have to travel within the buildings or reflects off of the surrounding building. The reference intersection has different building structures at each corner. This provides us the opportunity to investigate the impact of individual corner structure on the RSS and PER metrics. We do not directly account for the buildings. The impact is rather captured by different parameters fitted for individual corners.

The Region of Interest (ROI) is divided to five sub-regions; Four intersection legs and an intersection box. All of the transmission/reception/location log entries are assigned a location tag. These tags along with the buildings' 2D coordinates in the area are used to execute the *NLOS Test*, wherein if the line between the locations of the TX and RX locations intersects with at least one of the building edges, then that packet transmission is tagged as NLOS.

Vehicular Traffic. As previous work in the literature show, surrounding vehicular traffic impacts the pathloss component as well [21, 25]. However, the available data about the ongoing vehicular traffic during our experiments was not sufficient to neither directly account for obstructing cars to calculate a link-level impact, nor to categorize the available dataset based on grouped traffic conditions. Therefore, an average impact of the vehicular traffic is captured in the dataset, as the field experiments have covered different commuting times in different days.

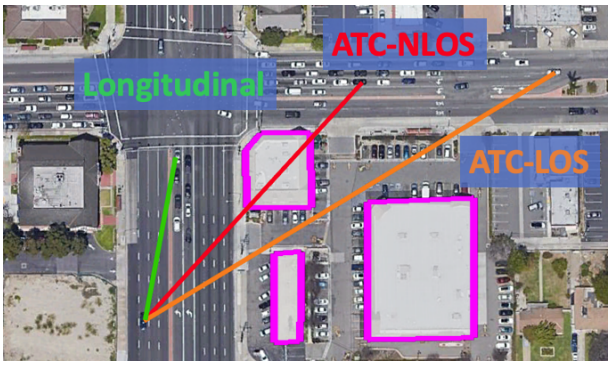

Figure 2.5: Recognized V2V links by our proposed model.

2.4 Propagation Models

We explore a hybrid propagation loss model based on distance measures. For finer resolution, we separately model Longitudinal propagation (i.e., propagation in the same intersection leg or across continuous legs), and Around-the-Corner (ATC) propagation (i.e., propagation across orthogonal legs).

Figure 2.5 shows the different type of links that are accounted for in the proposed model. We assume that the simulator has access to the road geometry and can recognize ATC links based on the location of both transceivers. We further assume that it can perform a *NLOS Test*, by checking whether the line between a transmitter and receiver intersects with building outlines in the area. If it does not intersect with buildings, the link is classified as *ATC-LOS*, otherwise it is categorized as *ATC-NLOS*.

2.4.1 Longitudinal Propagation

We approximate longitudinal propagation with a log-normal model. In logarithmic scale, the received power is modeled as given by Equation 2.3.

$$P_{rx} = P_{tx} - A_{lng} - 10B_{lng}\log_{10}(d_{tx-rx}) + Y + X_{\sigma} \tag{2.3}$$

Here, A_{lng} is the intercept and it models the pathloss at a close distance to the receiver. B_{lng} is the pathloss exponent and it models how rapidly the power decays over transmitter-receiver distance of d_{tx-rx}. X_{σ} is a zero-mean normal random variable with σ_X standard deviation and Y is an autoregressive process with σ_Y^2 marginal

variance, reflecting a stochastic component accounting for dynamic obstructions and fading sources on the road. We briefly explain how we fitted Y and X_σ in the following subsections.

We obtain the parameters for our model by setting up an optimization problem where we minimize the error between the mean/median received power produced by our model and the median RSS observed in the field experiments. We employ MATLAB's `fminsearch` function which uses the simplex search method. Once minimized, the remaining error, or Root Mean Square Error (RMSE), is used to fit X and Y as discussed in 2.4.3. For higher accuracy, the fitting process is applied to the North-South and East-West propagation separately, rather than a combined model for all available Longitudinal propagation samples.

2.4.2 Around-the-Corner (ATC) Propagation

For ATC propagation, the relative placement with respect to the intersection is a significant factor in addition to the transmitter receiver distance. To model this with a stochastic approach, we explore the following alternative distance measures:

- d_{tx-rx}: The distance between transmitter and receiver.
- d_{tx-0} and d_{rx-0}: distances between transmitter and the center of the intersection, and receiver and the center of the intersection, respectively.
- $d_{tx-axis}$ and $d_{rx-axis}$: distances between transmitter and the passenger-side curb, and receiver and the passenger-side curb, respectively, as heuristics to capture the lane number.

It is not surprising that for some of the distance measures combinations we obtain similar performance, as many of the distance measures depend on one another and thus, the effective amount of input information remains the same. After considering different combinations of the above distances, Equation 2.4 showed a better fit for the

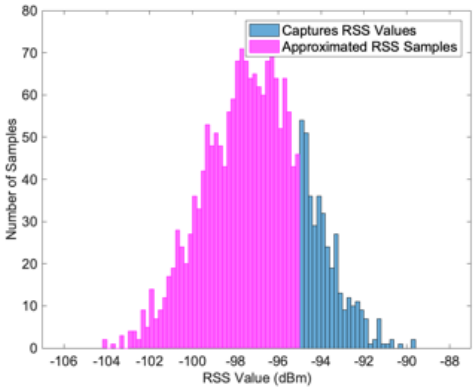

Figure 2.6: An example of regenerated RSS distribution for one of the 2D distance bins.

ATC propagation.

$$\begin{aligned} P_{rx} = P_{tx} - A_{ATC} &- 10B_{ATC}\log_{10}(d_{tx-rx}) \\ &- 10C_{ATC}\log_{10}(d_{tx-0}) \\ &- 10D_{ATC}\log_{10}(d_{rx-0}) \\ &+ Y + X_{\sigma} \end{aligned} \tag{2.4}$$

At first, the fitted model showed much lower attenuation. We believe that it was caused by most of our data lying near the Receive Power Threshold (-95 dBm). This means that there are many lost packets for which we were unable to capture the RSS. By bringing the data samples closer to the observed mean, we are diverging from the true mean of the model, which would be composed of the observed and the censored RSS samples. During parameter fit procedure, we learned that without accounting for the lost samples the fitted model would not show a good accuracy.

To tackle this problem, we account for the lost packets due to lower RSS, the whole 2D distance range, i.e. transmitter distance to the center of intersection and receiver distance to the center of intersection, are binned. For each 2D bin, which we call it a *tile*, the Packet Error Ratio (PER) is calculated. For the bins where PER is less than 30%, the standard deviation of RSS values is calculated and averaged across all tiles with the same condition. The acquired standard deviation is further used to approximate RSS distribution for other 2D bins where the PER is less than 90%. The reason for ignoring the tiles with more than 90% of packet loss is that there are too few samples to start with to recreate signal strength distribution for that tile.

The ATC fitting process is analogous to the Longitudinal case; that is, by setting up the error minimization optimization problem and solving it with MATLAB's `fminsearch` method. For finer tuning, the fitting process is applied to the North-West, South-West, North-East and South-East propagation cases whenever the *NLOS Test* was positive for the packet transmission in post-processing (ATC-NLOS). Only one set of parameters, however, is extracted for ATC when the *NLOS Test* is negative (ATC-LOS). We do not distinguish between different corners for ATC-LOS propagation. Table 2.2 shows the fitted parameters for ATC and Longitudinal propagation.

Table 2.2: **Model Parameters**

	Case	**A**	**B**	**C**	**D**	σ
Arount-the-Corner	North-East	4.464	2.411	1.567	1.569	4.38
	South-East	-25.782	2.238	0.963	0.955	4.57
	South-West	-2.327	1.008	2.298	2.346	4.75
	North-West	6.958	0.116	2.889	2.921	4.43
	LOS	-34.958	1.815	0.726	0.660	7.42
Longitudinal	South-North	-30.909	2.972	-	-	5.72
	East-West	-31.117	2.983	-	-	5.66

2.4.3 Accounting for the Residual Fading

One way to capture the Root Mean Square Error (RMSE) from the distant-dependent pathloss component calibration is to define one normal random variable to regenerate the calculated RMSE. This will result in high variation for a single wireless link by mistake, since the dataset used for the calibration is aggregated samples from many different experiment iterations, each with their own channel condition properties such as traffic condition. Therefore, we introduce two random variables: 1) A correlated random variable Y by using a fitted autoregressive (AR) process for a typical wireless link from the dataset, and 2) a normal random variable X to capture the residual variance around the fitted Y. Equation 2.5 and 2.6 calculate σ_X, i.e. residual standard deviation of X based on the marginal variance σ_Y^2.

$$\sigma_Y^2 = \frac{\sigma_w^2 \times (1 - \phi_1)}{(1 + \phi_1) \times (1 - \phi_0 - \phi_1) \times (1 + \phi_0 - \phi_1)} \tag{2.5}$$

$$\sigma_X = RMSE - \sigma_Y \tag{2.6}$$

Where σ_w^2, ϕ_0 and ϕ_1 are fitted parameters of Y.

2.5 Simulation Results

To validate our proposed model, a version of ns-3 simulator [26] that was previously calibrated for V2V environment [27, 28] is used. For a fair comparison, mobility trajectories of the test cars are extracted from experiment log files and simulation parameters are set just as they were in the field experiments. Table 2.3 shows experiment and simulation parameters. The extracted mobility trajectories have been further fed into the simulator to generate log files similar to those from the field experiment.

Table 2.3: Experiment Configuration

Parameter	**Value**
DSRC Message Rate	20 Hz
Packet Size	$\sim$ 135 Bytes
Transmit Power	20 dBm
Total Cable Loss	6 dB
Antenna gain	0 dB
DSRC Channel	172 (5855-5865 MHz)
Position Update Interval	100 ms

2.5.1 Simulation Accuracy

To quantitatively evaluate the performance of the proposed propagation loss model, the packet error ratio (PER) is arguably a key metric because driving safety applications depend on successful packet reception. Therefore, higher level application metrics heavily depend on accurate PER simulation. Equation 2.7 calculates simulation accuracy for each tile, i.e. a 2D distance bin for the distance of the TX and RX to the center of the intersection.

$$\begin{cases} E^{i,j} = |\frac{PER_{sim}^{i,j} - PER_{exp}^{i,j}}{PER_{exp}^{i,j}}| \times 100 \\ E_b^{i,j} = min(E^{i,j}, 100) \\ A^{i,j} = 100 - E_b^{i,j} \qquad\qquad i,j \in \mathbb{N} \end{cases} \tag{2.7}$$

Here i and j are the indices of different distance bins of TX and RX from the center of the intersection. In the first step, the relative error between PER values from simulation

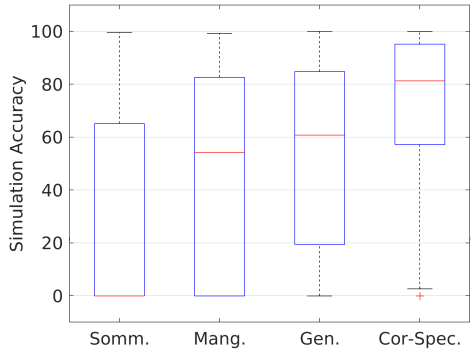

Figure 2.7: Distribution of simulation accuracy in terms of PER for different models: Somm. = Sommer et al., Mang. = Mangel et al., Gen. = The proposed model fitted for the entire ATC-NLOS dataset, and Cor-Spec. = The proposed model with corner-specific set of parameters.

($PER_{sim}^{i,j}$) and PER values from experiment ($PER_{exp}^{i,j}$) is calculated for all i's and j's. As the calculated relative difference can be potentially more than 100%, the value is bounded using $E_b^{i,j}$ before calculating accuracy values of $A^{i,j}$.

One challenge is to determine which 2D distance bins should be considered for performance evaluation, as PER gets very close to one after either TX or RX are in a relatively short distance into the intersection legs. One way to decide is to leverage the context, i.e. V2V safety applications in this case. As majority of crash scenarios at intersections happen closer to the center, we decided to calculate $A_{i,j}$'s up to 140 m for both of TX and RX distances to the center of the reference intersection.

For performance evaluation purposes, we selected models introduced and fitted by Sommer et al. [22] and Mangel et al. [24] as propagation models frequently used for intersection environment in the literature [23, 29]. For a thorough evaluation, we compare simulation accuracy of the aforementioned models to two different configurations of our proposed hybrid propagation model. In one configuration, labeled as *Cor-Spec.* (or C), four different set of parameters are fitted using the collected ATC data for each of the four corners of the intersection. In addition to our Corner-Specific configuration, we also provide simulation results for a configuration where our entire ATC-NLOS communication dataset is used to fit the model's parameters, regardless of the corner. This configuration is considered a more generalized model, labeled as *Gen.* (or G). Note that in both configurations, the simulator distinguishes between Longitudinal and

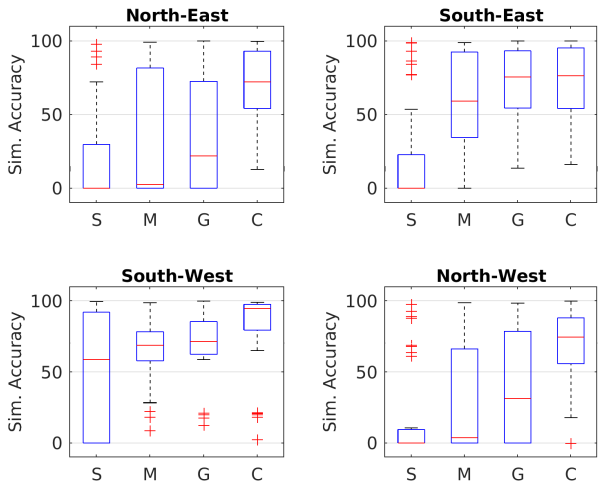

Figure 2.8: Distribution of simulation accuracy evaluated for individual corners by: S = Sommer et al., M = Mangel et al., G = The proposed model fitted for the entire ATC-NLOS dataset, and C = The proposed model with corner-specific set of parameters.

Around-the-Corner propagation.

Figure 2.7 shows the distribution of the calculated simulation accuracy for 2D distance bins, accounting for the distance of the TX to the center of the intersection and the distance of the RX to the center of intersections for bin size of 20 m. The figure shows that our model outperforms both baseline models by at least 25% better simulation accuracy. We believe the accuracy difference between the two configurations of our model shows that the structure of the buildings at specific corners of an intersection has a very high impact on the propagation, as there is ≈40% accuracy difference between the two. The model introduced by Sommer et al. does not match the measurements well. The PER accuracy median of zero indicates that at least half of the PER tiles have a value that differs more than 100% from the corresponding PER values captured in our experiments.

To better understand the impact of different building structures on signal attenuation, we further evaluated simulation accuracy for individual corners. Note that only model labeled as *C*, i.e. the corner-specific configuration of our proposed model, is able to distinguish between different corners, and other models use similar parameters for all corners. The first observation from Figure 2.8 is that the proposed model outperforms the baseline with better median and 25^{th}% values for all corners. Among all the

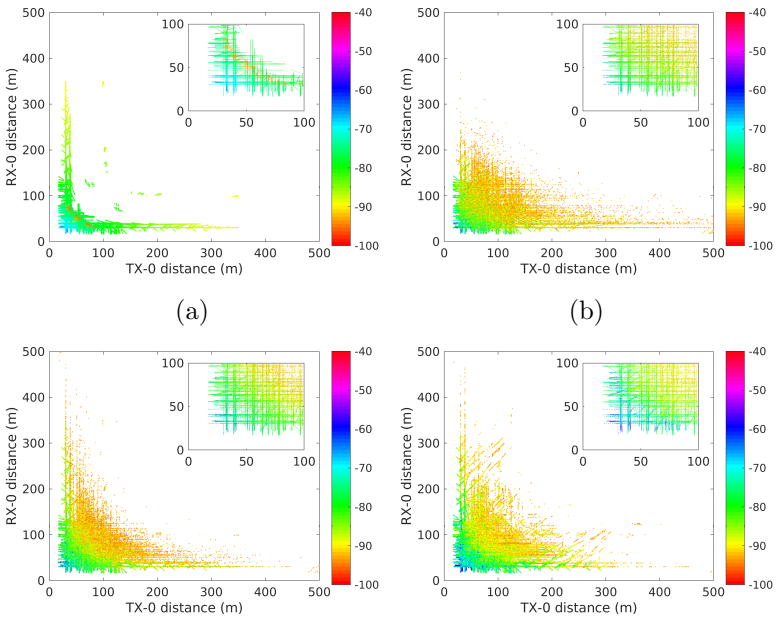

Figure 2.9: Received Signal Strength (RSS) comparison for the North-West corner between (a) baseline model by Sommer et al., (b) baseline model by Mangel et al., (c) our proposed model with corner-specific parameters, and (d) experiment data.

corners, the North-East and the North-West corners look challenging for both baseline and the generalized version of our model. The baseline shows simulation accuracy for these two corners with a median close to zero. This means the difference between the calculated PER for the field experiments and simulations is $\geq$100% in comparison to experiment's PER for at least 50% of the tiles.

The primary reason for such simulation inaccuracy, i.e. large relative differences between field experiment and simulation PER values, in the absence of interference is inaccurate signal strength calculation at the receiver. This is caused by uncalibrated propagation loss model. Such inaccuracy becomes more problematic, resulting in even more PER inaccuracies when hundreds or thousands of nodes are engaged in the simulation around the intersection, where interference becomes one of the sources of packet loss. Therefore, the magnitude of accuracy in scenarios with lower chance of interference can potentially grow for realistic simulation with many nodes.

2.5.2 Corner-Specific Metric Comparison

As Section 2.4.2 indicated, the ATC propagation can not be easily captured by only the distance between TX and RX. With the same logic, we chose to illustrate RSS and PER metrics for different distances of TX and RX to the reference point, i.e. the center of intersection in this context.

Let us compare Received Signal Strength (RSS) of received packets for experiment with propagation models discussed before. In Figure 2.9 each colored-dot represents an RSS value for a received packet. The values of X and Y axis for each RSS sample shows the distance of its transmitter to the center of intersection and the distance of its receiver to the center of the intersection, respectively. By comparing Figures 2.9c and 2.9d, it is seen that the range of packet reception and the color shade of the RSS values follow the captured samples from experiments. On the contrary, none of the baseline models can capture the trend of Figure 2.9d.

As for the Packet Error Ratio (PER) Figure 2.10 shows 2D PER values for different TX-0 and RX-0 distance bins, where the bin size is 20 m. In this figure, experiment results (shown in the first row) are compared to simulation results (shown in the second row) using our proposed model with corner-specific configuration. It is observed that the proposed model can adapt well to the slope of the pathloss, which can be more for some corners (SW in Figure 2.10) and less for some others (NE in Figure 2.10).

2.6 Discussion

One observation from Figure 2.9 is that the RSS distribution over TX-0 and RX-0 is almost mirrored regarding line x = y for the experiment results. We believe such balanced RSS distribution is caused by the scenario setup where all of the test cars are transmitting and receiving at the same time. Therefore, for each BSM with $d_{tx-0} = d_1$ and $d_{rx-0} = d_2$, there exists another BSM with $d_{tx-0} \approx d_2$ and $d_{rx-0} \approx d_1$ with time difference less than 50 msec (test cars transmit at 20 Hz).

Acknowledging symmetry as one of the basics of wireless signal propagation characteristics, the model by Sommer et al. and our proposed model seem to reflect such

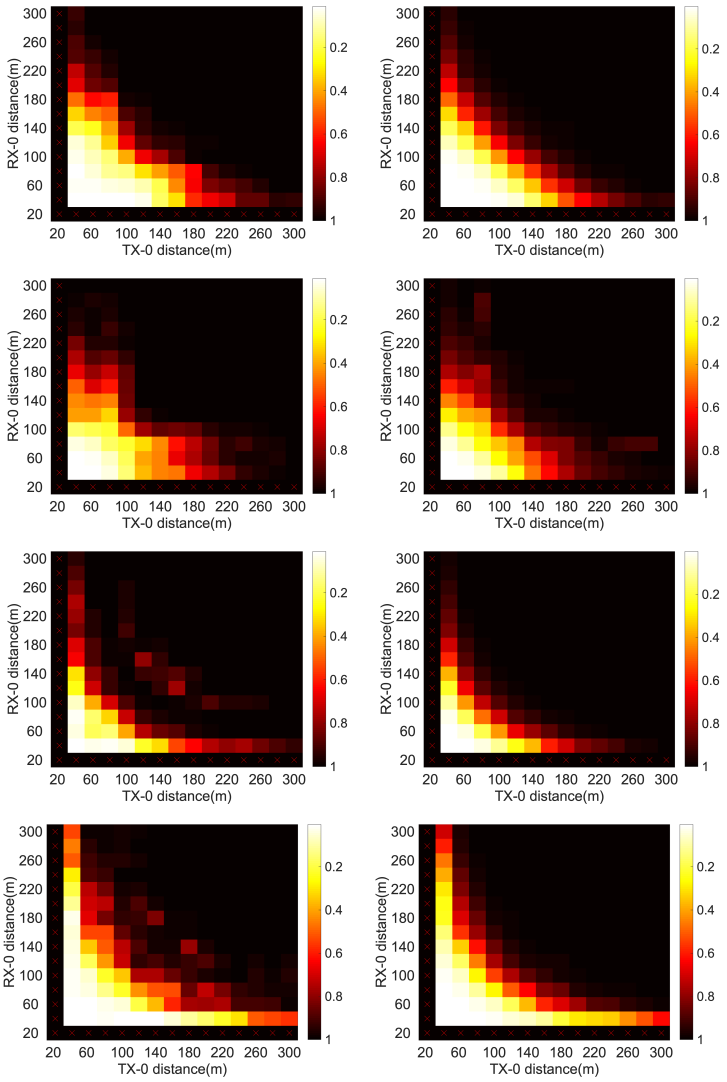

Figure 2.10: Packet Error Ratio comparison between experiment data (1st column) and simulation results with the proposed model (2nd column) left to right, for North-East (1st row), South-East (2nd row), South-West (3rd row), and North-West (4th row).

property (see Figures 2.9a and 2.9c). Quite the contrary, the Model by Mangel et al. seems to fail capturing the essence of channel symmetry (see Figure 2.9b). We believe such phenomenon is caused by differentiating between geometrical location of TX and RX regarding buildings' walls in Equation 2.2.

2.7 Conclusion

In this chapter we report our experience from a large-scale data collection with 10 DSRC transceivers in an intersection with real vehicular traffic. We used near-production

DSRC radios and Basic Safety Message (BSM) to exchange information on channel 172. The collected data is further analyzed, resulting in a scalable hybrid propagation loss model that is both geometrical in terms of using building geometry to distinguish between LOS and NLOS, as well as stochastic because the impact of buildings and ongoing vehicular traffic on propagation behavior is captured implicitly by different parameters of a stochastic model. We showed that individual building structures have significant impact on propagation at different intersection corners, so that a stochastic model with separate parameters for each corner outperforms an average model over all corners. We also find that existing intersection models do not fit the experimental data well. Simulations show that the proposed model achieves 80% accuracy on average in terms of PER, with a 25% to 80% improvement over models suggested by previous studies.

2.8 Chapter Summary

In summary, the contributions of this chapter are as follows:

- presenting and analyzing experiment data, collected from a busy intersection with real vehicular traffic and state-of-the-art DSRC radios.
- proposing a hybrid propagation accounting for buildings' shadowing by different path loss exponent values, as well as distinguishing LOS and NLOS cases per packet transmission.
- cross-validating simulation results using field experiment data and illustrating the resulting accuracy using physical and network layer metrics such as Packet Error Ratio (PER) and Received Signal Strength (RSS).
- comparing simulation results using the proposed model and comparable propagation loss models for intersection from the literature.

2.9 Acknowledgment

I thank the CAMP VSC6 Team and the United States Department of Transportation (USDOT) and the National Highway Traffic Safety Administration (NHTSA) for

planning and executing the requisite tests, providing the measurement data as well as sponsoring the work that enabled the channel model analysis. The CAMP VSC6 Consortium consists of the Ford Motor Company, General Motors LLC., Honda R&D Americas, Inc., Hyundai-Kia America Technical Center, Nissan Technical Center North America, and Volkswagen Group of America. Steve VanSickle was the Principal Investigator for the project. The experiments were designed based on discussions with CAMP VSC6 colleagues as well as S M Osman Gani, Ehsan Emad Marvasti, MD Saifuddin, and Dr. Yaser P. Fallah from the University of Central Florida.

2.10 Disclaimer

The opinions, findings and conclusions expressed in this chapter are those of the author(s) and not necessarily those of the USDOT or the NHTSA. The United States Government assumes no liability for its content or use thereof.

Chapter 3

Pedestrian-to-Everything (P2X) Simulator Design

This chapter aims to describe primary components of a calibrated simulator for P2X communication. It starts by analysing pedestrian-involved accident scenarios, and then describes the steps to generate a realistic Manhattan mobility trace for pedestrians. At the end of this chapter, the channel model used in the simulator are described.

3.1 Pedestrian-Vehicle Accident Scenarios

According to a study conducted by NHTSA in 2014 [30], a traffic accident involving pedestrians is the result of numerous factors including limitations in road geometry, excessive traveling speed of a vehicle, adverse weather, and visual obstruction of human drivers. These factors together lead to delayed or missed detection of a pedestrian. This can be mitigated, as estimated by the study, by equipping vehicles with extra detection capabilities for pedestrians. In the context of this thesis, we focus on such capabilities provided by DSRC, where pedestrians carry devices sending DSRC packets to vehicles. We hope that P2V communications can alert the driver or vehicle to the presence of a pedestrian sufficiently in advance to avoid possible traffic accidents.

In particular, we are concerned with the performance of P2V communications in the two scenarios shown in Figure 3.1. These scenarios represent almost 67% of the total pedestrian fatalities as highlighted in [31]. In the first scenario, a vehicle moves straight with a pedestrian walking against/along traffic. Here, the pedestrian might visible or obscured by other traffic. In the second scenario, a pedestrian could be hidden by objects (e.g., corner of a building), leaving not enough time for the vehicle to brake once detected. These two scenarios require P2V communications work within both LOS and NLOS environments in order to eliminate traffic accidents.

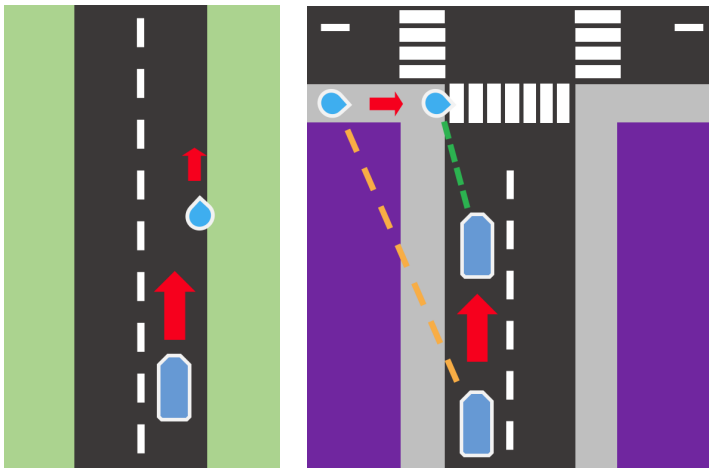

(a) (b)

Figure 3.1: General pre-crash scenarios: (a) moving along/against traffic; (b) crossing road

The case for early awareness is further supported by the recent SAE J2945/9 document [31], which indicates 8 seconds before collision as the time requirement for issuing a situation awareness message. Therefore, it is possible that a pedestrian who will cross the street is still on the sidewalk, hidden behind a building from the perspective of the approaching car. Motivated by this consideration, we separately model and analyze line-of-sight and non-line-of-sight communication links in the simulation.

3.2 Case Study and Simulation Scenario

We selected the Times Square neighborhood in New York City because of its particularly high pedestrian and vehicle density and harsh wireless signal propagation environment, when compared to most other United States locations. It therefore represents a challenging scenario for pedestrian to vehicle communications because the performance of a P2V link depends not only on the channel propagation environment but also on the aggregate interference from other transmitters. It is also a location that faces pedestrian safety challenges. In a 2015 city government safety action plan [32], it has been identified as one of the priority intersection, which require further action to reduce pedestrian accidents. Manhattan overall accounts for 34 out of an average 157 annual New York City pedestrian fatalities.

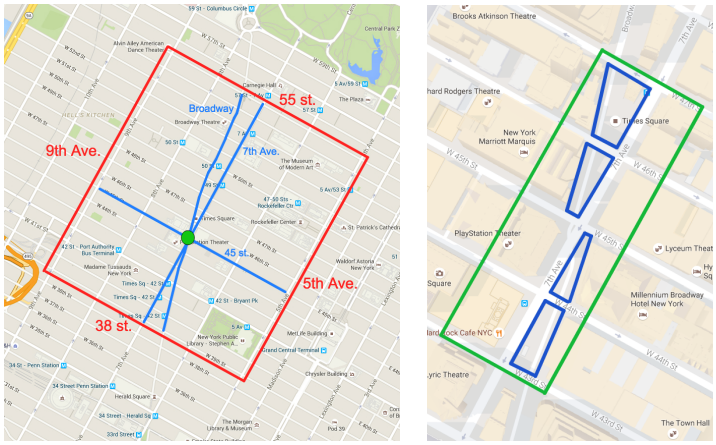

(a) (b)

Figure 3.2: (a) The area and roads with simulated pedestrian and vehicle traffic (b) Location of stationary pedestrians within Times Square

Figure 3.2a shows the area we used to create the scenario's topology. Since we focus on examining network parameters at the center of Times Square (i.e. green dot in Figure 3.2a), the expected point of peak channel load, the selected dimensions are chosen to encompass the maximum interference range in the simulation scenario.

To keep the number of simulated nodes within a computationally feasible range for ns-3, we used a heuristic to further limit the pedestrians represented in the simulator to those that can actually significantly contribute to the channel load at the center of Times Square and impact the system performance. The path loss exponent between a pair of transceivers that are located on two different sides of a building is very high (see Section 3.3). This means that the spatial channel load for two parts of the map with a building between them are almost uncorrelated. We therefore retained only generated pedestrian and vehicle traffic in immediately adjacent streets (the area within the green box in Figure 3.2b) and for the roads where line-of-sight to the center of Times Square exists (marked by blue in Figure 3.2a).

The pedestrian and vehicle traffic traces are generated using the SUMO mobility simulator [33]. The resulting mobility traces, are further calibrated using more than three hundred photos we took during peak hours in the area. SUMO generates vehicle and pedestrian movement traces using Origin-Destination models. The primary model

(a) Taken Between 46 St. and 47 St. looking south

(b) Taken at 48 St. and 7th Ave. intersection, looking north

Figure 3.3: Sample photograph footage used to validate the simulated mobility traces

uses a graph representation of the map, where vertices and edges represent intersections and streets, respectively. Then entities such as pedestrians and vehicles can be generated for a pair of origin and destination edges. The density and general movement pattern can be further controlled by manipulating parameters such as the maximum walk distance, the probability of origin and destination edges at the map's margin, etc.

Given the goal to evaluate channel load and interference, we focused on matching the overall distribution and movements of pedestrians in a short, say 10s simulation. Since we do not require long simulation times, we did not attempt to create accurate origin-destination models for pedestrian trips. Figure 3.3b is an example photo used to calibrate the density of moving pedestrians by providing number of pedestrians waiting for green traffic light to pass a particular intersection in the aforementioned map. We adjusted the pedestrian traffic flow parameters in the SUMO simulator until the count at the same intersection in the mobility trace approximately match the one obtained from the photo.

In the Times Square area marked by dark blue in Figure 3.2b, most pedestrians linger and do not move for periods of time. Those pedestrians are not well-represented by SUMO default models. We therefore decided to create 400 additional pedestrians

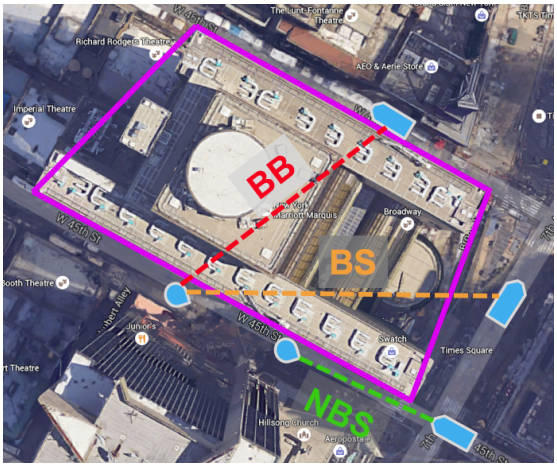

Figure 3.4: Different link types between transceivers

in Times Square, which are modeled as stationary given our short simulation time. We used photos such as Figure 3.3a to match the distribution and the number of stationary pedestrians in Times Square, between 44 Street and 47 Street.

Note that only the movement for pedestrians and vehicles which are outdoors is modeled; people inside buildings, and vehicles parked in indoor parking areas are not included in the mobility traces even though they could also contribute to interference, albeit at somewhat lower levels due to building attenuation.

The resulting scenario comprises approximately 400 vehicles and 2000 moving pedestrians across 7th avenue, 45 Street and Broadway, and 400 stationary stationary pedestrians at peak time across Times Square. [1]

3.3 Propagation Environment

To better reflect the propagation environment in a densely-built urban environment, we designed the simulator to choose different models depending on the degree to which the direct path is obstructed between a sender and receiver. The simulator maintains a map of building outlines (obtained from OpenStreetMap) and uses these to distinguish three situations: No-Building Shadowing (NBS), Building Shadowing (BS), and Building Blocked (BB). Figure 3.4 illustrates these link categories. From a simulation perspective, whenever there is a packet transmission, the propagation loss module

[1] The mobility traces and ns-3 simulator source code are available for download [34].

within the simulator identifies the matching category for the link and then calculates the received signal according to the corresponding propagation model. We describe the exact selection criteria and models next.

Table 3.1: Propagation Environment Summary

Name	**Link Type**	**Preliminary Loss Model**	**Final Loss Model**
NBS	No Building Shadowing	Log Distance model with parameters in [24]	Longitudinal model described in Chapter 2
BS	Building Shadowing	Proposed loss model in [24]	The ATC model described in Chapter 2
BB	Building Blocked	Constant infinite loss	Constant infinite loss

Table 3.1 summarizes different links categories based on the relative transceiver and and building's locations. Note that the model described in Chapter 2 was developed in a separate line of work as this thesis was shaping. Therefore, the results showed in Chapter 4 and Chapter 5 are generated using the preliminary propagation loss model. However, we regenerated some of the key results of Chapter 6 with the calibrated model of Chapter 2.

No Building Shadowing (NBS) Links: If the direct path between two transceivers does not intersect any of the building edges, then the link is classified as not being affected by building shadowing and blocking. An example of NBS links is shown in Figure 3.4 where the link color is green.

Building Shadowing (BS) Links: If the line is intersecting two adjacent edges of the same building, then the link between them is considered as a wireless link with building shadowing, where the two transceivers share an intersection that they have LOS access to its center. We label this category of links, which is showed with yellow color in Figure 3.4, with BS.

Building Blocked (BB) Links: The third category is where the link between two transceivers is blocked by a building. But, in this case, the two transceivers do not share an intersection, i.e. they are located in parallel streets (see the red color link in Figure 3.4). Considering the height and depth of the buildings in Manhattan area, we assumed the signal strength on the other side of the building would be negligible

and the interference is not accounted for in the simulation. If there is more than one building between the transceivers, the link is considered as BB as well.

3.4 Chapter Summary

To summarize, the contributions of this chapter are:

- Reviewing primary pedestrian-vehicle accident scenarios with the highest probability.
- Designed, introduced and validated a challenging high-density mobility scenario for pedestrian safety message evaluations.
- Introducing the propagation model to be used in the P2X simulator.

Chapter 4

Congestion Control in P2X Communication for Idealized Positioning Accuracy

4.1 Idealized Candidate Contextual Transmission Policy (CTP)

For the sake of clarity, let us first ignore possible measurements errors and consider a CTP for operation under ideal conditions.

The first context rule of the algorithm eliminates transmissions when the smartphone remains stationary for a longer period of time t_s, a time interval which would be configured on the order of several minutes. Vulnerable road users usually move and very rarely sit or remain stationary for an extended period of time. In contrast, smartphone users inside buildings, restaurants, or cafes may sit or put aside their smartphone for longer periods of time. Modern smartphone contain low-power inertial sensors that can efficiently track such movement, further motivates this baseline rule.

When motion is detected, the transmission policy uses inertial techniques to determine the type of motion (walking, running, bicycle, in-vehicles, train) using algorithms as discussed in prior work [35]. The CTP will transmit PSMs when walking, running, and bicycle transportation modes are detected but not for vehicle or train occupants, which are not considered vulnerable road users (and vehicles are expected to have their own DSRC transmitters). When running or bicycle modes are detected, the transmitter can remain in higher-risk mode (i.e. more frequent transmission) due to the higher speeds involved and the shorter duration of such activities compared to time spent walking.

The primary challenge then lies in assessing risk in the walking context. The walking context may be further refined by using indoor/outdoor classification techniques [36], in

which case transmissions can be disabled indoors. These algorithms generally consume more power than movement detection, which motivates their use as a secondary algorithm that is only periodically active when a user is walking. Note though that complete deactivation of indoor transmissions may create risks in indoor parking garages.

Ideally, the walking context should also be further refined by using in-street context information, since the majority of pedestrians usually moves in relatively safe sidewalk or pedestrian plaza locations. With ideal sensor and map information, the CTP could use the VRU's location to examine if the VRU is located on the road simply by comparing the most recent GPS location L_{latest} reported by the smartphone, with the borders of nearby sidewalks and streets. To perform such a comparison, L_{latest} would need to be accurate to about one meter. Moreover, a carefully calibrated map is required, where boarders of streets and sidewalks are accurately marked. There are two primary challenges with the aforementioned method: 1) Many electronic maps define streets only with their centerline and do not precisely delineate sidewalks. 2) GPS sensors on smartphones exhibit tens of meters of error in urban canyons. Therefore, a direct comparison between L_{latest} and road-sidewalk borders is unlikely to work. Since no sufficiently accurate in-street detection algorithm exist that can operate in dense urban areas and only rely on smartphone sensors, we focus the remainder of the discussion on this aspect.

While much of the DSRC effort has concentrated on allowing vehicles to exchange position information to enhance situational awareness, the recent SAE J2945/9 [31] standardization activities are also explicitly considering vulnerable road users, which includes pedestrians. We refer the reader to this standard document for further details on application scenarios and system design. Here we focus on the network congestion question. Addressing channel congestion and co-channel interference has already required significant work when only considering transmissions between vehicles [37, 38, 39]. This raises questions on how transmissions from potentially large numbers of pedestrians can be accommodated.

To explore and understand the scaling challenges inherent in pedestrian-to-vehicle communications, this chapter reports on an effort to evaluate the load generated and

the performance achieved in a particularly dense urban environment of chapter 3. We construct a simulation scenario for the neighborhood surrounding Times Square in New York City and generate pedestrian and vehicle traces using the Simulation of Urban Mobility (SUMO) simulator. These traces are then replayed in the ns-3 network simulator using different pedestrian transmission strategies. In particular, we consider update rates between 1 Hz and 5 Hz for each pedestrian. We also consider contextual triggers that activate and deactivate P2X transmissions based on whether the pedestrian is moving and whether the pedestrian is located in the street. We report the channel load as well as packet error and latency, in terms of the inter-packet gap achieved in this case study scenario.

4.1.1 Transmission Trigger Policies

We assume that the pedestrian transmission will be activated by a trigger policy since it is undesirable to contribute to channel congestion and handset battery drain when the user is in no need protection. By exploiting rich sensor data from a smartphone, the generation of VRU safety message can be context-based, i.e., the message generation is only triggered in certain situations that can be detected with smartphone sensors. Based on a review of relevant context-detection literature, we select three possible trigger conditions for further study. Note that the focus of this thesis is not on developing these context sensing technologies but to evaluate their effectiveness in contextual trigger policies, assuming that the sensing itself can be realized. Table 4.1 summarizes relevant context sensing technology.

Table 4.1: Sensing Technology Assumptions for Smartphones

Outdoor Environment Detection	The device is able to distinguish outdoor environments from indoor [40, 41]
Movement Detection	The device is able to detect movements, e.g. using accelerometer [42]
Approaching Road Detection	The device is able to detect crossing a road using, e.g. GPS or other sensors [43]
In-vehicle phone detection	The device is able to detect if it is in a vehicle [44]

Based on the technology assumptions in table 4.1, the considered VRU safety message transmission policies are:

Baseline (Outdoor): All pedestrians located outdoor periodically generates a safety message at fixed transmission rate r. Specifically, we consider rates of 1 Hz, 2 Hz, and 5 Hz. We selected those rates with the goal of enabling the receiver to track the position of a moving pedestrian. Lower rates would lead to considerable movement of a running pedestrian in between updates. Higher rates would not offer a tracking benefit considering expected pedestrian speed and achievable positioning accuracies. Note that indoor persons are not included in our simulations, since there normally is no risk of traffic accidents. We also assume that phones in vehicles do not transmit because vehicles are planned to have built-in DSRC transmitters.

MovingPed: This contextual trigger policy activates transmissions at the fixed rate r only when the pedestrian is outdoor and moving. Transmissions begin immediately when movement is detected and continue for a time window S after the phone last senses movement. Mobile smartphones in vehicles are assumed not to transmit.

Multiple Tx Rates: This algorithm allows all outdoor pedestrians to transmit but at different rates depending on whether they are stationary or moving. Moving pedestrians transmit at the faster 5Hz rate and stationary pedestrians transmit at the slower 2Hz rate. Again, mobile smartphones in vehicles are assumed not to transmit.

On-StreetPed This policy only allows pedestrians that are located on streets to transmit at a fixed rate r. Sensing technology to support such distinctions is less mature than movement and in-vehicle detection but we include it here for reference since knowing about such pedestrians is presumably more relevant to vehicles than the many pedestrians that are safely located on sidewalks.

4.2 Evaluation

To evaluate channel load, test-bed implementation would be very expensive regarding the scale of the scenario. Instead, we use ns-3.16 [26] with Wifi frame capture [45] to simulate the communication between pedestrians and vehicles. The list of simulation

parameters is given in table 5.1.

Table 4.2: Simulation Parameters

Parameter	**Value**
CW_{min}	15
AIFSN	2
Packet size	316 bytes
Data rate	6 Mbps
Transmission power	20 dBm
Noise floor	-98 dBm
Energy detection thrshld	-85 dBm
Simulation time	10 sec

We use three metrics to evaluate simulation results: Channel Busy Percentage (CBP) as the indicator of channel load, Packet Error Ratio (PER) and near worst case Inter-Packet Gap (95% IPG). These are typical link quality parameters in the V2V safety communication research [35, 46]. CBP is calculated using Eq. 5.3.

$$CBP = \frac{t_{ChBusy}}{t_{CBP}} \times 100\% \tag{4.1}$$

Where t_{CBP} is the CBP measurement window and t_{ChBusy} is the time period during which the channel is measured as busy by the device. PER is the ratio of the number of dropped messages to the sum of the received and dropped messages for each pair of transmitter and receiver. Likewise, IPG measures the time between two consecutively received packets between a pair of transmitter and receiver. IPG is an important performance metric since it determines how frequently a vehicle could get information updates, such as the location, from a particular pedestrian. The near worst case analysis for IPG helps to understand how bad the system might perform.

The PER and 95% IPG are calculated based on the transmissions carried out in Times Square area (the green box in Figure 3.2b). That is, if the transmitter is within the green box the transmission is accounted for computation regardless of whether the receiver is within the same region or not. Since vehicles are probably less interested in getting updates from a pedestrian located on a parallel road (not opposite lanes on the same road), where there is a building between them, all the BB links are excluded. The distance between transmitter and receiver determines in which distance bin the

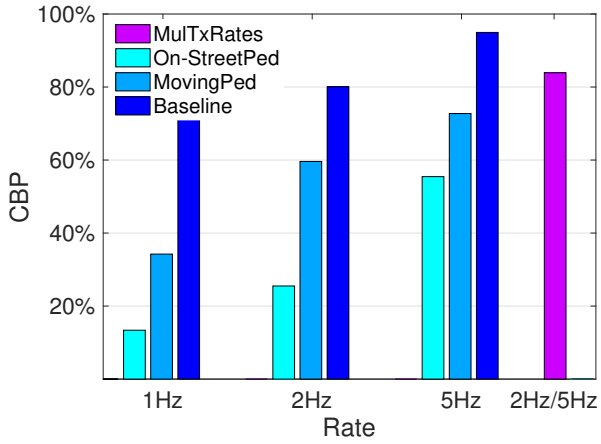

Figure 4.1: Measured CBP at the center of Times Square

transmission (successful/unsuccessful) is counted. The distance bin is set to 30 meters in this work.

Figure 4.1 shows average CBP over 10 seconds of simulation for different rates and different transmission trigger policies at the center of Times Square (green circle in Figure 3.2a). The simulation initialization phase, further, has been removed from the calculations. Since, so far, there is no standard on the issue of the VRU safety message generation rate, all the performance and channel load evaluations are done where the VRU safety message transmission rate r is 1 Hz, 2 Hz, or 5 Hz, which means that VRU safety messages are transmitted every 1 second, 500 milliseconds or 200 milliseconds, respectively, once the policy's constraints are met. As Multiple Tx Rates (labeled as *MulTxRates* in the figures) is a policy using both 2 Hz (Stationary pedestrians) and 5 Hz (Moving pedestrians). Its results are shown separately with the single bar.

While the argument against lower safety message transmission rates is that they simply might not meet the minimum safety requirements regarding the location updates, Figure 4.1 shows that the channel easily gets saturated when the frequency of safety message transmission grows. On the other hand, the baseline transmission policy shows worst performance. Simulation results show 94% as CBP for Baseline $r = 5Hz$ due to transmissions of hidden nodes from different streets, which is high enough to saturate the channel. MulTxRates holds the second busiest channel among other policies and rates with CBP 84%.

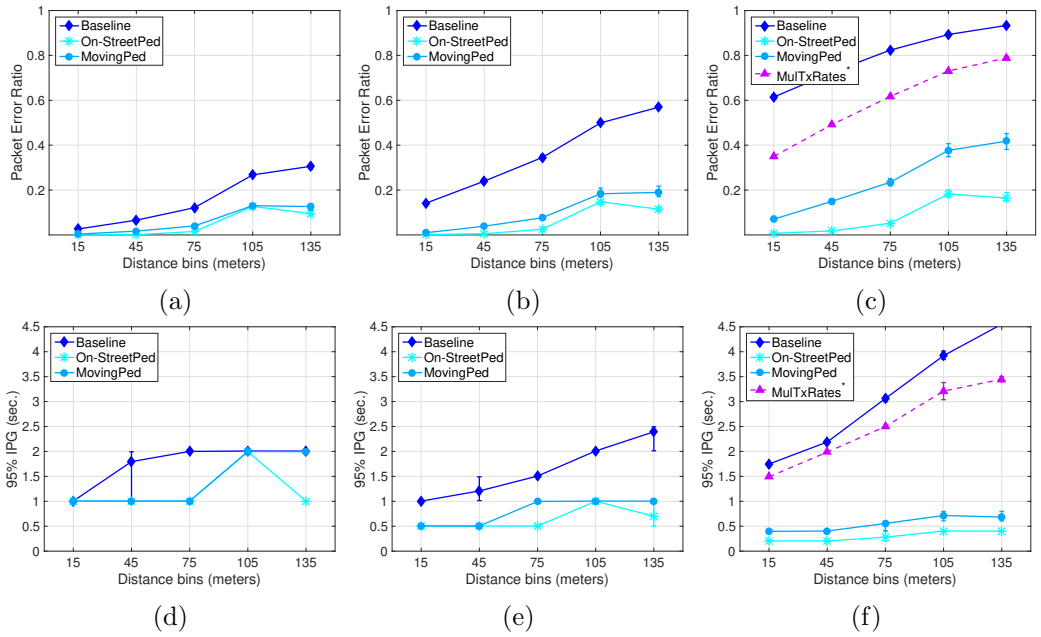

Figure 4.2: PER and 95% IPG analysis for NBS and BS links: (a) PER for $r = 1Hz$; (b) PER for $r = 2Hz$; (c) PER for $r = 5Hz$ (d) 95% IPG for $r = 1Hz$; (e) 95% IPG for $r = 2Hz$; (f) 95% IPG for $r = 5Hz$
* Stationary pedestrians transmit at $r = 2Hz$ and moving pedestrians transmit at $r = 5Hz$

Figure 4.2 shows performance metric analysis based on simulation results. Each metric calculation in this figure is averaged on five simulation runs with different mobility traces. The error bars on each distance bin result represent minimum and maximum over all five simulation runs.

Figures 4.2a-4.2c show PER for different VRU safety message transmission policies where the transmission rates are $r = 1Hz$, $r = 2Hz$ and $r = 5Hz$, respectively. For each of these PER plots, the corresponding 95% IPG results are presented in Figure 4.2d-4.2f. It can be seen that the PER increases dramatically where no transmission constraints are used other than the outdoor detection. Figure 4.2f shows that a high PER for Baseline can further lead to undesirable IPG results. Normally, the higher the 95% IPG, the less reliable the system is.

Some of the PER and 95% IPG results for 135m are lower than at 105m distance, which seems surprising. In the simulation logs, we found that the 105m bin contains more samples from BS links, which has worse communication performance than NSB links, than the 135m bin. We believe that this is an artifact of the building layout in

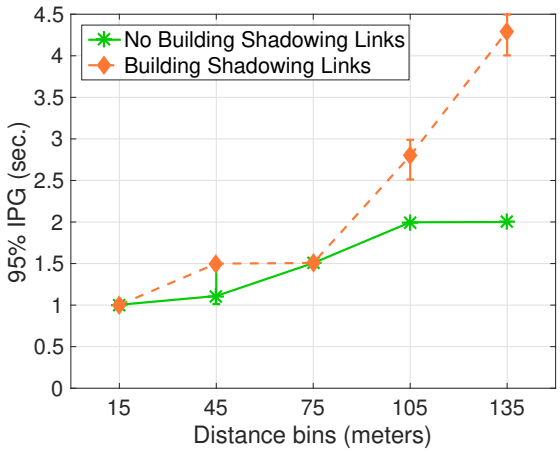

Figure 4.3: 95% IPG for Baseline $r = 2Hz$ for different link types

this particular environment.

Another observation from Figure 4.2 is that the system is significantly more reliable as the given transmission rate increases up to 5 Hz when MovingPed or On-StreetPed used. This is also consistent with the observation from Figure 4.1, where the channel is not optimally used, suggesting that there could be even more packets on the air in a given time interval. Not surprisingly, MulTxRates still has the second worst performance among all rates/policies.

Although the presented results in Figure 4.2 for some of the transmission trigger policies are promising, note that performance analysis is done for the overall PER and 95% IPG in terms of different link types. As briefly mentioned in Section 3.1, there might be some special cases of the crossing road pre-crash scenario where the pedestrian is not in the driver's sight at the time that the first situation awareness transmission is needed to be delivered to the vehicle. In such cases, if the VRU safety message is delivered once the pedestrian moved to a LOS situation, the situation awareness alert time requirement specified in SAE J2945/9 might not be met before estimated TTC [31].

This is why we further split the results shown in Figure 4.2e based on the type of the wireless links at the time of communication. Figure 4.3 compares the 95% IPG for NBS and BS links. The figure shows a 40% to more than 100% jump in 95% IPG for the BS links in comparison with the NBS links at higher distance bins, where the

system functionality might mostly rely on BS links.

4.3 Related Work

Existing work in the VRU safety literature can be divided into four categories: 1) Sensor-based stand-alone approaches for smartphones; 2) Sensor-based stand-alone approaches for cars; 3) Collaborative approaches using infrastructure; 4) Ad hoc collaborative approaches.

The WalkSafe project [6] is an example of stand-alone applications that uses smartphone camera input to alert the pedestrian if any vehicle is approaching while the pedestrian is using the phone (i.e., talking while walking). In the same category, Jain et al. [43], introduce a new method to alert pedestrians who walk while using their phone whenever they step into the street. This method uses wearable sensors on the pedestrian's shoes paired with the smartphone to detect stepping into the street and can display an alert on a distracted pedestrian's smartphone screen. The presented method is introduced after the authors showed that GPS measurements provided by the smartphones in urban environments are not accurate enough to rely on [47]. These approaches focus on distracted pedestrians, and in their stand-alone form are not a general pedestrian safety solution.

Sensors mounted on vehicles, on the other hand, have potential to detect most pedestrians on the road. Research (e.g.,[48, 49]) that has used different vehicle-mounted sensors such as cameras, RADAR and LASER scanners falls into the second category. While this approach can detect pedestrians that are not using phones and not equipped with special devices, they work only if line-of-sight to the obstacle is available.

In the third category, as briefly mentioned before, Masud et al. [7] used an RFID tag based communication between pedestrians and cars around intersections via infrastructure equipment (i.e., road side units). While this study shows improved safety, the infrastructure requirement makes it harder to deploy. Sugimoto et al. [50] conducted a pedestrian to vehicle prototype study using 3G cellular communication and IEEE

802.11b WLAN technology. Another paper [51] also describes cellular-based communications between cars and pedestrians, but does not provide any reliability analysis due to high latency in the cellular network in comparison with wifi. Nowadays vehicular communication systems, however, are based on IEEE 802.11p [52]. David and Flach [53] introduce the idea of communication between cars and pedestrians where not all the pedestrians transmit all the time. Since the decision of which pedestrians and cars are at accident risk needs to be made in a server, the system has scalability and other drawbacks of centralized systems.

In 2013, Wu et al. [54] envisioned a future for DSRC technology that supports vulnerable road users such as pedestrians. This work focuses more on the handset battery consumption of the application. Wu et al. further conducted a test-bed study to analyze a Wifi-based P2V communication scenario [55]. While this study includes similar scenarios as those that motivate our research, none of this work has analyzed channel load and scalability of the system. Anaya et al. [56] analyzed some aspects of P2V communications such as the minimum distance required by each party to be successfully warned if the relative speed between the vehicle and the pedestrian is within a threshold. The wireless protocol used in their test-bed, however, is not IEEE 802.11p, which is considered for DSRC communications.

4.4 Discussion

Let us briefly discuss channel choice implications of these results and the impact of frame capture in these simulations.

4.4.1 Channel Choices

To enable vehicle to pedestrian communications, decision have to be made around the world on which channels to permit transmissions from mobile handsets. The simulations in this work have only considered pedestrian transmissions on a 10 MHz/6 Mbps DSRC channel with no other traffic. The channel load and performance results therefore best

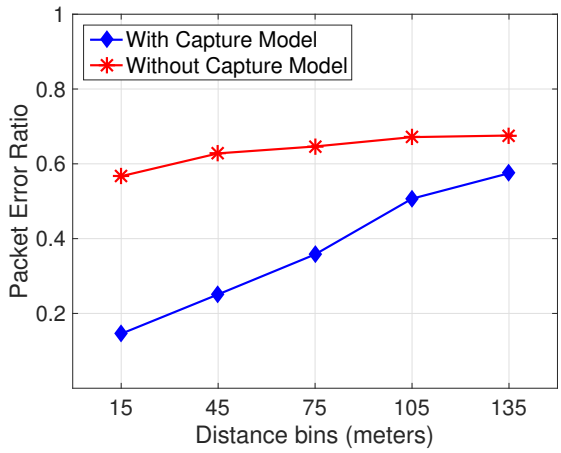

Figure 4.4: PER for Baseline $2Hz$, with/without wifi frame capture feature in the simulator

represent the results obtained with a dedicated channel for pedestrian to vehicle communications, which is separate from all other DSRC-related messaging. Receiving such messages would then require an additional radio in cars that is tuned to this channel. One might also ask whether such messages can be accommodated on the safety channel used for vehicle-to-vehicle safety messaging. Given the relatively high channel loads obtained even with contextual triggers for moving detection, it is questionable whether a 10 MHz channel offers enough capacity for both vehicle and pedestrian messages. It is possible, though, that future work will lead to improved sensing strategies that can identify particularly dangerous traffic situations involving pedestrians, which could allow for such transmissions.

4.4.2 Impact of Frame Capture Implementation

Frame Capture is a feature of modern wireless chips that allows switching to receiving a newly arrived signal with a stronger signal strength when a reception of a weaker signal was already in process. While to date, the official release of the ns-3 simulator does not support this feature, we implement the frame capture effect in our simulator by applying patches we have developed [45]. To emphasize the importance of the capture effect model in these simulation studies, we repeat some of the experiments with the default ns-3 packet reception model (i.e., without frame capture).

Figure 4.4 compares the PER where the simulator is using the default ns-3's packet reception model with simulator using wifi frame capture. All the other simulation settings and the scenario configuration are kept. Note that the simulation results show up to 40% increase in PER when the default ns-3 packet reception model is used. This is mostly because at short distance bins, the wifi frame capture feature is able to lock to a stronger frame coming from a nearby device. On the contrary, the default ns-3 packet reception model drops both the currently receiving packet and the newly arrived packet.

4.5 Conclusion

We first created a simulation scenario for Times Square area in New York City and generate pedestrian and vehicle traces using the Simulation of Urban Mobility (SUMO) simulator. These mobility traces were further replayed in the ns-3 network simulator to evaluate channel load and performance of such a network. The evaluation is done considering sample transmission trigger policies that prioritize moving pedestrians or on-street pedestrians where the transmission rate is varying between 1 Hz and 5 Hz. Extensive simulation results show that results for the 5 Hz transmission policy, where the smartphones transmit at 5 Hz when an outdoor environment is detected (Baseline policy) raise questions on whether vulnerable road user performance targets can be met in crowded environments. It also has been shown that there exists significant potential to improve the network performance through context-aware transmissions policies or trigger conditions.

4.6 Chapter Summary

To summarize, the contributions of this chapter are:

- Network performance and channel load evaluations for different transmission policies and update rate assumptions.

- Showing that the the network performance can be significantly improved via contextual transmission policies, such as those prioritizing moving or in-street pedestrians.

Chapter 5

Reducing Unnecessary P2X Safety Transmissions Using a Proximity-Based Heuristic

Many VRUs move in inherently more safe locations, such as a sidewalk, where the risk of colliding with a vehicle is very small. Other pedestrians, for example those crossing the street, are at higher risk and information about them is significantly more valuable to nearby vehicles for safety applications. Existing congestion control algorithms, mainly developed for V2V environment, do not account for this and would lead to relatively uniform reductions in message rate over all pedestrians. Naively applying them here could lead to unnecessary transmissions from pedestrians that are safe and potentially too few transmissions from pedestrian at risk.

To address this challenge, this work proposes a Contextual Transmission Policy (CTP) for VRUs based on a smartphone sensor-based classification algorithm to detect when VRUs are on the road. The CTP is orthogonal to the congestion control algorithms and can be viewed as a prioritization strategy that maintain high rates for pedestrians at risk but seeks to reduce unnecessary message transmissions from those who can be determined to be at very low risk. To assess risk, the classifier uses several contextual parameters such as movement and type of motion but primarily relies on location of the VRU. It estimates the VRU distance from key crossing points, locations that are frequently used by pedestrians to cross the street. Since Global Positioning System (GPS) readings are frequently inaccurate in urban canyons, where the error is more than tens of meters, the algorithm uses additional guard zones around these crossing points based on positioning error estimates. If the VRU is located sufficiently far away from the crossing point at the road border, that is outside the guard zone, the VRU is judged at low risk and assigned a low message rate. The guard zone is

determined adaptively based on GPS error estimates to maximize the reduction of the unnecessary PSM transmissions while not missing any VRUs that cross the street.

While CTP is compatible with different communication architectures, the simulation implementation and evaluation assumes Dedicated Short Range Communication (DSRC) technology, which enables low-latency message transmissions. A full implementation could build on smartphone prototypes capable of transmitting PSMs that have been demonstrated by industry [57].

5.1 Background

Recent activities from the Intelligent Transportation System (ITS) community demonstrated growing interests in using wireless communication to improve the safety of VRUs. For example, the Volpe National Transportation System Center (NTSC) analyzed the national crash database and prioritized pre-crash scenarios that lead up to traffic accidents involving pedestrians and vehicles [58]. The project helps lay the foundation to develop new wireless communication-based pedestrian-to-vehicle (P2V) cooperative safety applications. Meanwhile, the US Department of Transportation (USDoT) funded the city of Tampa in Florida through its Connected Vehicle Pilot program to explore a proof-of-concept P2V solution [59]. The goal of the effort is to provide a safer traveling experience for pedestrians at intersections. Further, a working group of the Society of Automotive Engineers (SAE) recently worked to publish a P2V communication standard J2945/9 [13] which defines a set of preliminary technical specifications for using the Dedicated Short Range Communication (DSRC) technology to transmit PSMs. This standard will serve as a guidance for manufactures to build devices supporting P2V communications in the U.S.

5.1.1 A Contextual Approach

The above analysis highlights the need to pursue a new PSM-oriented congestion control solution. A promising research direction is to understand VRU safety context and focus transmission of PSMs more on the critical moments where such a message is

necessary. This direction, given the above discussion, could enable an algorithm to reduce both battery consumption for a VRU device and congestion on the wireless channel. In our previous work [60], we have demonstrated that if the pedestrian's contextual information can be collected accurately, it could help significantly reduce the communication traffic load over the channel.

To extract pedestrian's contextual information, prior work has focused on using data from smartphone's built-in sensors. Our previous work [43, 47, 61] have studied the feasibility and limitations of using built-in sensors to identify pedestrian risk scenarios. In [47], we analyzed the performance of positioning and inertial sensing techniques for in-street pedestrian detection in both rural and urban scenarios. Further in [61], we demonstrated the data obtained from multiple sensors (e.g. GPS, gyroscope, compass, etc.) on the smartphone can be explored to detect pedestrian's movements, such as turning left or right, and then predict when the pedestrians are about to cross the street. However, both work identified that the performance of the proposed detection techniques can get potentially affected by the high-rise buildings in the urban area due to large errors in the positioning.

To tackle the positioning challenges, we created a new detection technique based on shoe mounted inertial sensors which can characterize pedestrian's on-ramp walking and the process of stepping down from a street curb without fine-grained GPS information [43]. Although the performance of the system was demonstrated encouraging, the requirement of additional shoe-mounted inertial sensor may limit the large-scale deployment of the system.

Tang et al. [62] proposed an algorithm to detect street crossing attempts of pedestrians by using images from their smartphone camera. The algorithm detects distracted pedestrians who cross a street while using a phone, e.g. texting. However, this algorithm requires pedestrians to hold their smartphones while walking, which may not be the case in many situations. Bujari et al. presented in [63] an algorithm which leverages the accelerometer on the smartphon to detect street-crossing events after pedestrians waited for the green phase of a traffic light. The algorithm was cost effective. However, unpredictable human behavior lead to a high false positive and negative rates.

This chapter pursues an approach that relies on the sensory data on the smartphone to extract pedestrian's contextual information without any special interaction between the smartphone and the pedestrian. The information is further used to develop a CTP that sends PSMs for a pedestrian based on his/her perceived safety level. Our design goal for the CTP is to reduce the transmission of PSMs as much as possible without compromising the safety of a pedestrian.

5.2 Contextual Transmission Policy

The key idea of the proposed CTP is to track multiple context clues that indicate that a smartphone user is not currently a vulnerable road user and to reduce or eliminate personal safety message transmission in this case. In particular, the design focuses on the key challenge of identifying the many smartphone users who are in relatively safe location on sidewalks or in pedestrian zones even when the positioning data available to the smartphone is affected by errors on the order of tens of meters, as frequently the case in urban canyons. It accomplishes this through a map of common street crossing points, where pedestrians walk onto the street, and an adaptive guard zone around these crossing points that is adjusted based on the positioning error estimate.

5.2.1 CTP with Walking Risk Assessment

Without access to the detailed map and accurate location of VRUs, the proposed design uses a proximity heuristic, to compare VRU's noisy GPS location with the locations where VRUs frequently cross the street. Such crossing points, C_i, can be manually marked on a map stored in the phone, or can be potentially determined automatically by overhearing the positions reported in others' PSMs over a longer span of time. The rationale is that if a pedestrian is in proximity of any such crossing point, there is a higher chance of crossing the street. Conversely, if the pedestrian is sufficiently far away from these crossing points and the risk of a mid-block or random crossing is low, the frequency of PSM transmissions can be reduced. Generally, the algorithm is intended to be conservative, it errs on the side of classifying pedestrians as $HighVulnerable$

while still located on the sidewalk rather than putting vulnerable pedestrians in danger by misclassifying them as safe.

More precisely, as shown in Algorithm 1, the CTP's main part (line 5-15) executes only if the VRU is moving/walking. Otherwise, the VRU is marked $LowVulnerable$. In our work, the accelerometer on smartphones is used to analyze VRU movement which, once detected, triggers the algorithm to update the proximity threshold d_{Thr} (line 4), as discussed later. Then, the classifier algorithm calculates a distance d_i between the latest reported location L_{latest} and each nearby crossing location C_i from the map, where $i = 1, 2..N$ and N is the number crossing points stored in the phone's map within a predefined radius around the device. If the condition $d_i < d_{Thr}$ is satisfied for at least one i, then the VRU is marked as $HighVulnerable$, otherwise as $LowVulnerable$.

Algorithm 1 Proximity-Based CTP Algorithm

```
1: Input: C_i, L_latest, err_{L-latest}, w_max
2: Output: Vulnerability level
3: if VRUIsMoving then
4:     d_Thr ← maximum(α × err_{L-latest}, w_max)
5:     for Crossing point C_i do
6:         d_i ← distance between L_latest and C_i
7:         if d_i ≤ d_Thr then
8:             mark this VRU as HighVulnerable
9:             return
10:        end if
11:    end for
12:    if RandomCrossingDetection then
13:        mark this VRU as HighVulnerable
14:        return
15:    end if
16: end if
17: mark this VRU as LowVulnerable
18: return
```

The key to addressing positioning inaccuracies lies in the choice of the threshold d_{Thr} which defines a guard zone around the crossing points. While a fixed, conservative d_{Thr} would simplify the algorithm, we consider an adaptive threshold to address the changing GPS error magnitude over time. The algorithm monitors the GPS error $err_{L-latest}$ reported by the smartphone[1] and multiplies it with a safety coefficient α

[1]Android, for example, provides the `getAccuracy()` method, which returns a floating point number

to obtain d_{Thr}. Note though that the street-width w_{max} should be a lower bound for d_{Thr}. The maximum nearby street width w_{max} can be obtained from maps such as OpenStreetMap [65] or could potentially be calculated using differences between nearby crossing points C_i.

To accommodate possible mid-block crossing and stepping into the street at other random locations, the algorithm can incorporate additional heuristics (line 12-15). First, stepping off a curb results in larger acceleration measurements than regular steps [43]. Second, in areas with sidewalks, stepping off the curb other than at an intersection is often preceded by a change in direction, which can be monitored using inertial sensors on phones. The algorithm should revert to $HighVulnerable$ classification when such conditions are detected. This is indicated in the algorithm with the $RandomCrossingDetection$ condition (line 12).

5.3 Evaluation

We study the risk classification accuracy and the impact of the CTP algorithm on network performance using a simulation model spanning several blocks around Times Square in Manhattan with pedestrian movements generated using the SUMO traffic generator.

5.3.1 Evaluation Metrics

To measure how well the proposed CTP classifier can detect the VRUs crossing streets, we select Recall and Specificity metrics. Recall is defined as:

$$Recall = \frac{TruePositives}{TruePositives + FalseNegatives} \tag{5.1}$$

A greater Recall value indicates that more pedestrians who are crossing the street have been correctly classified as $HighVulnerable$. To err on the side of safety we choose a minimum threshold of 95% for Recall. Parameter choices that led to Recall values below this threshold, were not further evaluated.

---

indicating the radius of 68% confidence for the phone's position [64].

Instead of Precision, Specificity is considered the secondary criterion. Specificity, or the true negative rate, directly represents the ratio of outcomes that correctly classifies VRUs on the sidewalk, which better reflects our goals. The Specificity is defined as:

$$Specificity = \frac{TrueNegatives}{TrueNegatives + FalsePositives} \tag{5.2}$$

A greater Specificity value indicates a higher true negative rate, i.e. more pedestrians who are safely walking on the sidewalk were correctly classified as such. Higher Specificity means that more unnecessary PSM transmissions can be avoided. Specificity is therefore another indirect indicator of energy efficiency.

Network Performance

We evaluate the impact on network performance in terms of the channel busy percentage, packet error rate, and information age. Since we focus safety applications, the PER and Information Age calculation only considers transmissions where the transmitter is actually at risk (in the street) as determined by ground truth simulator data.

Channel Busy Percentage (CBP) rises with channel load and very high CBP is undesirable because it degrades communication performance due to higher chances of collision. It is defined in Eq. 5.3.

$$CBP = \frac{t_{Busy}}{t_{CBPwindow}} \tag{5.3}$$

where $t_{CBPwindow}$ is the CBP measurement window and t_{Busy} is the time period during which the channel is considered as busy by the simulator.

The Packet Error Rate (PER) combines errors due to low received signals (large distance) and due to collisions. To allow separating these, we calculate PER separately for different transmitter-receiver distances using 30m distance bins. In our simulations, the PER is calculated based on the transmissions carried out in Times Square area (the red box in Figure 5.2). That is, if the transmitter is within the red box the transmission is accounted for, regardless of the receiver location.

The Information Age reflects how fresh the pedestrian's information is at the receiver [66]. The information age is the time since the last successfully received message,

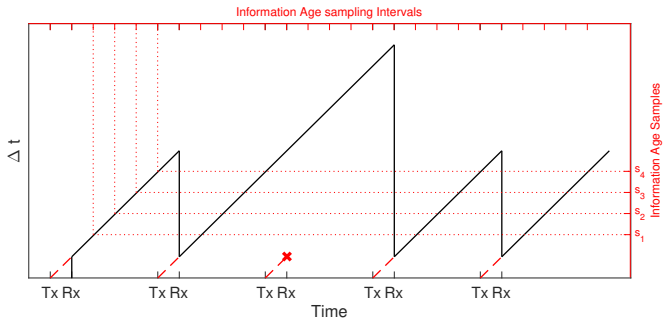

Figure 5.1: Communication between two transceivers and Information Age sampling over time

which contains the last position update from the pedestrian. To illustrate this, Figure 5.1 shows a time diagram for communication between two transceivers. The information age increases linearly with time and resets to zero every time a message is successfully received. The simulator samples information age periodically, illustrated by samples 1-4 shown on the right side of Y axis. We further calculate the cumulative distribution function (CDF) of these values over all transmitter-receiver pairs where the transmitter is a VRU located on the street and transmitter-receiver distance is less than 150 meters. Information age increase when unnecessary transmission lead to channel congestion due to the associated collisions. It also increases when an in-street VRU is misclassified since this reduces the message rate of that node. It therefore reflects overall CTP performance.

We also report the total number of transmissions by all the VRU devices during 85 seconds of simulation, which is approximately proportional to the energy overhead of these techniques. The proposed CTP, VRU devices neither need to communicate with each other nor receive information from vehicles. They can operate in TX-only mode, fall back into power-save modes immediately after each transmission.

5.3.2 Simulation Setup

The proposed classifier and its impact on network performance is evaluated by using the ns-3 simulator [26]. To generate more accurate results, the simulator is modified to implement frame capture [27, 45]. PSMs are broadcasted over one-hop on a 10 MHz channel at 5.9 GHz band. As for the path loss model, different models are used

depending on the link type between the transmitter and receiver at the time of the communication. If there is no building between the pair, a log distance model plus Nakagami fading is used. If at least one building is in between, but the locations of the pair are on different legs of the same intersection, then the proposed loss model of [24] is used. Finally, if the pair are located on parallel street with at least one building in between them, then it is assumed that the packet is lost due to the attenuation from the structure of the building. More detail can be found in chapter 3. Table 5.1 shows important simulation parameters.

Table 5.1: Simulation parameters

Parameter	**Value**
$t_{CBPwindow}$	200 msec
CW_{min}	15
AIFSN	2
Packet size	316 bytes
Data rate	6 Mbps
Transmission power	20 dBm
Noise floor	-98 dBm
Energy detection thrshld	-85 dBm
Channel bandwidth	10 MHz
GPS error model	Gaussian dist. $\mu = 20$ m
Simulation time	90 sec

Since the performance of the proposed classifier depends on the position information reported by the GPS devices, an urban canyon environment is considered as the simulation scenario due to its challenging signal propagation situation for GPS signals. Figure 5.2 shows the neighborhood around Times Square in New York city. The movements of cars, pedestrians, and bicyclists are simulated by SUMO [33]. The aforementioned model has been extended from work [60] in that the mobility traces are simulated for every road way highlighted in blue while retaining the focus on high node density around Times Square. Another reason for choosing Times Square neighborhood is its high density of pedestrians in the area which helps to evaluate network performance under a near worst-case network load.

The generated scenario includes approximately 400 vehicles, 2300 pedestrians, and

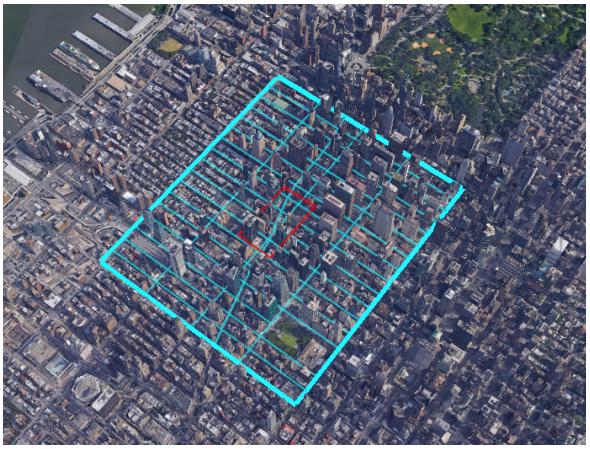

Figure 5.2: Simulation scenario map - Times Square, NY, USA

30 bicycles across 7th avenue, 45 Street and Broadway. Note that only pedestrians and vehicles which are outdoors are modeled, that is people inside buildings, and vehicles parked in parking areas are not transmitting and receiving PSMs. Also, we do not evaluate mid-block and random crossings because it is not supported by the SUMO mobility simulator used in this work and we do not yet have suitable location traces.

5.3.3 Algorithms and Baselines

Our CTP algorithm assigns $1Hz$ as PSM message rate to pedestrians which are classified as $LowVulnerable$, i.e. located on sidewalk, and $5Hz$ to pedestrians which are determined to be $HighVulnerable$.

We compare the achieved performance by the proposed CTP, with an ideal oracle classifier that relies on accurate simulator information and maps to determine whether a VRU is located in the street or on a sidewalk. In addition, a baseline algorithm where all pedestrians transmit PSMs at $5Hz$ is used.

5.3.4 Simplified GPS Error Model

The implemented GPS error model in this work is using a magnitude positioning error with Gaussian distribution with mean of 20 meters, and angle of the error with uniform distribution between 0-360 degrees. The error samples are assumed uncorrelated. While not ideal for the urban canyon environment, this model provides a first approximation

of expected errors. GPS measurements in urban canyons are distorted because of attenuation, multipath, and shadowing effects. Multipath occurs when signals from satellites bounce off buildings and reach the receiver's antenna via different paths where the traveling times for those paths are longer than that of the Line-Of-Sight (LOS) path. Attenuation and shadowing can block the LOS path. GPS error distribution under LOS reportedly follow a normal distribution or Rayleigh distribution with no correlation between samples [67]. Under Non-Line-Of-Sight (NLOS) the error depends mostly on the obstructions' structures [68]. Related studies report 20 meters average and up to 40 meters GPS error for urban environments [43, 69]. Real GPS measurement will be incorporated in future work.

5.4 Results

We begin with risk classification accuracy and then examine the impact on network performance. Note that all results have been obtained from five simulation runs with different mobility traces, each 90 seconds simulation runtime. The results are furthers averaged across all five runs where 5 seconds of transient state of each simulation has been excluded from the metric calculation. The error bars are showing the minimum and maximum values obtained across different simulation runs.

Figure 5.3 shows comparison between the Recall metric and the Specificity metric for the proposed proximity-based classifier for different d_{Thr} configurations. A trivial fixed proximity threshold is also examined, where $d_{Thr} = 10m$ in order to show the drawbacks of such approach. To plot this figure, the classifier decision is examined every 200 msec for all the VRU devices in the simulation. Then Recall and Specificity are calculated and collected for each interval. At the end, the collected values are further averaged across the simulation duration.

Note that 68% confidence for the reported GPS error by the device is not modeled when generating GPS errors in the simulations. Therefore, the CTP algorithm is simulated where $\alpha = 1$ and $\alpha = 2$. Moreover, in order to show the impact of movement monitoring before marking a VRU as $HighVulnerable$, two cases are considered for

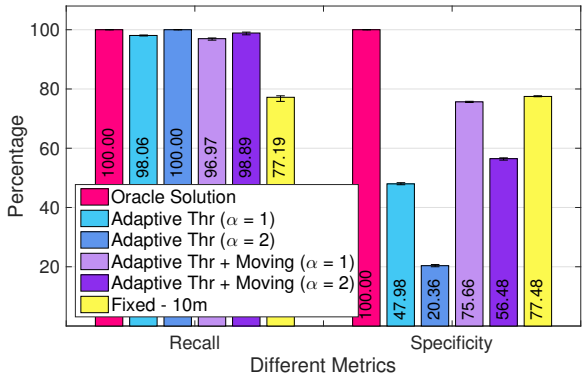

Figure 5.3: Classifier evaluation

simulation. The first case is where the CTP considers the movement as the prerequisite to be marked as $HighVulnerable$, labeled as $+Moving$, and when it overlooks the movement. All these configuration options result in four variations of CTP. These configurations are further compared with baseline and the Oracle Solution. Each figure includes a red bar/curve representing the Oracle solution as well as a bar/curve for the baseline where applicable.

The left side of Figure 5.3 shows the comparison of classifier's Recall. As expected, the Oracle solution has 100% Recall. The outlier, however, is the configuration where $d_{Thr} = 10m$. In this case, shown by the yellow bar, almost 25% of VRUs on the road are marked as virtually safe by mistake. The result is not greater than the threshold described in 5.3.1, as this type of wrong classification potentially puts the VRU's safety in jeopardy. Moreover, even if better results can be achieved by further optimizing the predefined fixed threshold, this solution is not reliable since in some challenging scenarios, e.g. in an urban canyon, GPS errors are time-varying and can be biased for several tens of meters [69]. Therefore, a constant threshold based solution, i.e. $d_{Thr} = 10m$, is incompetent in these scenarios and is not considered for further analysis.

As discussed earlier, we consider the Recall value of 95% as the minimum performance, which all of the four adaptive approaches can meet. This indicates that most of the VRUs who are crossing the street have been correctly identified by the proposed CTP classifier as $HighVulnerable$. The second priority is to reduce the cases where

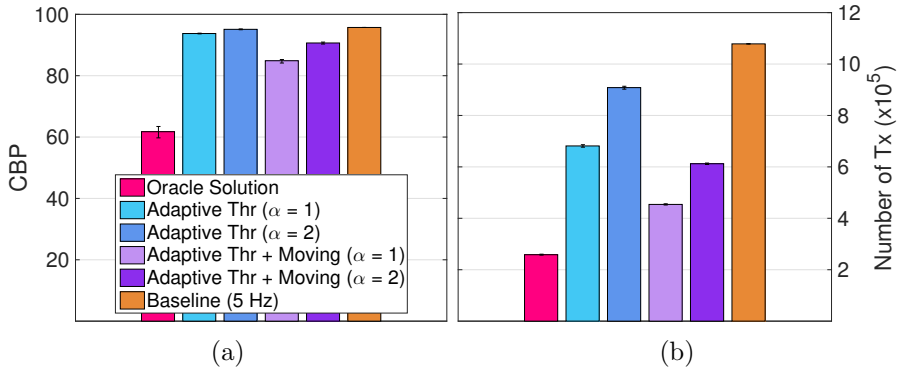

Figure 5.4: Channel load indicators; a) Channel Busy Percentage, and b) The number of transmitted PSMs during the simulation

VRUs in virtually safe situations are misclassified as $HighVulnerable$, i.e. VRUs located on the sidewalk are wrongly identified as in-street. Looking at the right side of Figure 5.3, we observe the configuration where $\alpha = 1$ and movement monitoring is applied, outperforms the other configurations with a degraded Recall value of 1-4%. The simulations results show that our classifier is able to achieve more 96% Recall and 75% Specificity.

Figure 5.4a shows the average CBP for different configurations of the proposed CTP. The CBP values are measured every 200 msec at the center of 7th avenue and 45th street intersection, and then are averaged over the simulation duration. Figure 5.4b shows the total number of transmissions sent by all the VRU devices in the simulation. We observe that although the total number of transmissions sent by VRUs differs from one configuration to another, the CBP values remain close to each other. For example, the difference of CBP values between baseline $5Hz$ and adaptive threshold using reported GPS as d_{Thr} is only 2%, but latter sends 50% more PSMs. This is because when the channel load is high, CBP values are no longer linearly (or near-linearly) proportional to the number of transmissions on the channel. Therefore, in these high channel load scenarios, the number of transmissions is a better indicator than the CBP for energy consumption. In general, the proposed CTP solution can reduce the number of transmissions by 15%-58% depending on the different configuration and different trade-off objectives. However, due to the very dense scenario of this work, the wireless channel is over-saturated and even reducing transmissions by half does not

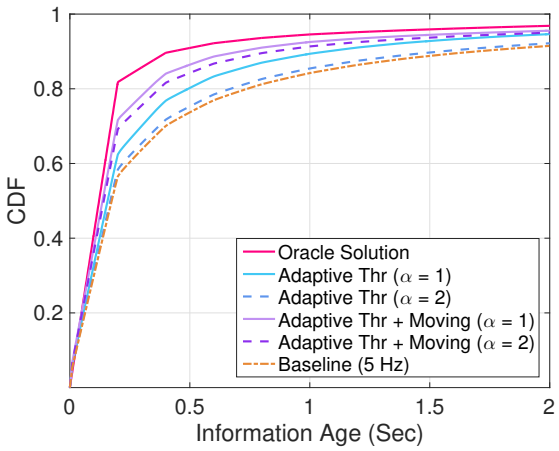

Figure 5.5: Information Age comparison for in-street VRUs

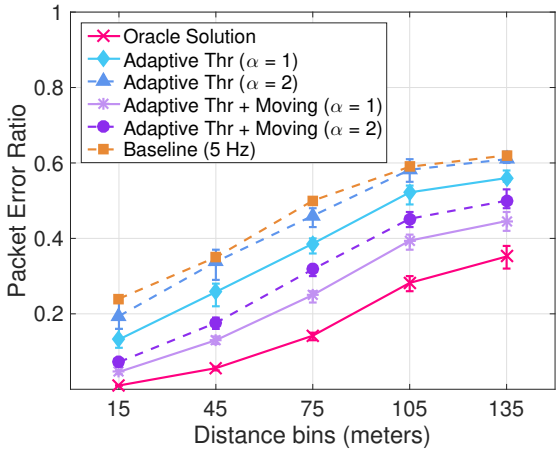

Figure 5.6: Packet Error Ratio comparison for in-street VRUs

mitigate the CBP as much.

Figure 5.5 shows the age of information contained as discussed in 5.3.1. The Information Age is sampled every 10 msec and the calculation is limited to the cases where the transmitter is a VRU in the street and is less than 150m away from the receiver. The observation is that with Oracle solution, about 90% of age samples are less than 440 ms. However, baseline 5Hz algorithm provides 1700 msec for the same criteria. As our CTP solutions, for the CTP configuration, where $\alpha = 1$ and the movement condition is considered, 90% of samples are less than 710 msec.

Such improvement when CTP is used is primarily because of the unnecessary transmission reduction that consequently reduces the packet collision on the wireless channel.

Figure 5.6 shows the calculated PER for in-street VRUs. The comparison between different CTP configurations and the baseline algorithms shows that our CTP solution with the configuration with $\alpha = 1$ and the movement condition checker can improve the PER up to 18%.

Since the distribution of GPS errors could potentially affect the results, a question may arise about the impact of the general accuracy of the GPS locations provided by smartphones on the proposed CTP algorithm performance. Table 5.2 presents the impact of the GPS accuracy on the CTP algorithm where the $\alpha = 1$ and movement checker is employed. The general observation is that the performance of the classifier is preserved with different levels of GPS accuracy assumptions. However, for the configuration that the reported GPS error is not compared with the maximum width of nearby streets in the process of adjusting d_{Thr} (look at the two rightmost columns), the Recall is degraded and the Specificity is improved as more accurate GPS locations provided. The main reason for this change is that the extremely low d_{Thr} values would not satisfy the distance comparison of line 5 in Algorithm 1. Consequently, many in-street VRUs are misclassified as $LowVulnerable$.

Table 5.2: Impact of GPS accuracy on CTP classifier performance

Classifier Conf.	μ_{err}	Comparing with Street Width?			
		yes		no	
		Recall	Spec.	Recall	Spec.
$\alpha = 1$ & Mov.	20 m	96.90	75.61	95.88	76.75
$\alpha = 1$ & Mov.	10 m	98.69	79.53	91.86	87.73
$\alpha = 1$ & Mov.	5 m	98.93	78.68	79.89	93.62

5.5 Discussion and Future Work

Further Congestion Mitigation. Note that after applying CTP the chosen message transmission rate can be further regulated through a channel congestion control mechanism. CTP primarily separates smartphones into distinct priority classes. The message rates assigned to each class could then be adjusted to the current channel load. To achieve this goal, one possible future step would be examining weighted message rate based congestion control algorithms such as Bansal and Kenney's work [70],

on top of the presented classifier. This could result in further improvements in network performance metrics.

Bicyclists with Smartphones. In future, some bicycles could also be equipped with a dedicated VRU device which can be activated when moving instead of simply relying on the bicyclist's smartphone to transmit PSMs. One remaining challenge would be avoiding duplicate transmissions from both the smartphone and the bicycle device. This can be resolved at the cost of higher energy consumption by making smartphones periodically listening to the channel and monitoring it for matching movement profiles, i.e. speed, heading, and location.

Energy Trade-offs. In our current design, smartphones are not assumed to listen to the channel to save energy. This allow their wireless chipsets to enter sleep mode while not transmitting. However, there is a trade-off in that it also causes the smartphone to miss information, for example about the presence of vehicles, which could also enable energy management techniques such as not transmitting when no vehicles are nearby. In the current simulation scenario, this would not have been effective since the scenario is so dense that there are a lot of cars in the communication range of every VRU in the scenario. More generally, though, this remains an interesting topic for future work.

5.6 Conclusions

In this chapter, we argued that the safety of Vulnerable Road Users (VRU), in particularly pedestrians, depends on their location more than their speed and designed a Contextual Transmission Policy (CTP) to account for this. While the overall CTP relies on multiple forms of context, we have focused on risk classification of pedestrians that are walking outdoors. To give priority to VRU's in the street, the CTP identifies potential in-street VRUs with a classifier that checks for proximity to common crossing points and can also incorporate additional crossing detection heuristics. VRUs that are potentially in the street maintain a higher message rate while those determined to be relatively safe off-street use reduced message rates. Simulation results show classifier accuracy of more than 96% Recall and 75% Specificity and an improvement in

information age from less than 1700 msec to less than 710 msec in 90% of the times.

5.7 Chapter Summary

To summarize, the contributions of this chapter are as follows:

- Introducing a contextual transmission policy that adjusts transmissions rate for VRUs primarily based on their location and can tolerate GPS positioning inaccuracies
- Evaluating the risk classification accuracy of the algorithm in a Manhattan-derived simulation model
- Examining the reduction in PSM transmissions and improvements in pedestrian-to-vehicle communication performance by applying the contextual transmission policy in a Manhattan simulation scenario

Chapter 6

A Multi-rate Congestion Controller for Pedestrian Communication

This chapter builds on this previous work [60, 71], presented in chapters 4 and 5, by proposing a multi-rate channel congestion control algorithm for a heterogeneous application environment, in conjunction with an example contextual transmission policy (CTP) to address the problem of the remaining congestion on the channel. The proposed CTP activates and deactivates Pedestrian-to-Everything (P2X) application transmissions by periodically examining whether the applications' requirements (say, positioning accuracy) can be met in the current environment. This can reduce message transmission rate when there is little benefit to such messages, for example when the current positioning accuracy is insufficient for applications to function. It also introduces message rate variations, however.

The focus of this chapter is therefore controlling the remaining congestion in the face of varying message rates. To cope with such a heterogeneous application environment, where various applications with different message rate requirements are operating on the same channel, the proposed multi-rate channel congestion controller functions as a gate-keeper in areas where channel congestion exceeds the limits allowable for safety applications. The proposed algorithm is further equipped with a cooperative channel busy monitoring mechanism to reduce smartphone energy consumption.

To evaluate this proposal, we use the simulator of Chapter 3. Note that the simulator includes a calibrated stochastic GPS error model [72] for this chapter's results. The simulation results show that the proposed framework and algorithms maintain the channel load near the target threshold as desired, resulting in information age (IA)

improvements for safety applications. They also show that the provided solution significantly reduces energy consumption on smartphones in comparison with the legacy CBP measurement mechanisms designed for V2V.

6.1 Background

Recent activities from the Intelligent Transportation System (ITS) community demonstrated growing interest in using wireless communication to improve the safety of vulnerable road users (VRU), such as pedestrians.

6.1.1 P2X Communication Initiatives

Recently, the USDOT funded three major pilot deployments across the US through its Connected Vehicle Pilot Deployment (CVPD) program to explore proof-of-concept P2X solutions [8] among other applications. The goal of P2X is to provide a safer traveling experience for pedestrians at intersections. The NYC CVPD [9], for example, includes two applications to enhance pedestrian safety: 1) a Pedestrian in Signalized Crosswalk Warning (PEDINXWALK), wherein road side units (RSUs) use sensors such as LIDAR to detect pedestrians in a crosswalk and notify oncoming vehicles about their presence over DSRC messages, and 2) a Mobile Accessible Pedestrian Signal System (PED-SIG) wherein the pedestrians smartphone listens to DSRC Signal Phase and Timing (SPaT) messages and MAP messages from an RSU at the traffic signal to assist visually impaired pedestrians in crossing the road (for example, by notifying them when the pedestrian signal allows crossing).

Wu et al. [55] introduce the first-of-its-kind pedestrian safety application based on vehicle-pedestrian communication. The paper explains steps taken to build a DSRC-enabled smartphone and further preparing the vehicle side radio for exchanging Basic Safety Messages (BSM). The authors indicate channel congestion as a primary challenge that needs to be addressed. Basic energy optimization is also introduced, for example by motion detection. Tahmasbi et al. [73] designed, implemented, tested and evaluated a similar vehicle-pedestrian system based on the SAE J2945/9 standard [13] and PSM.

The authors also discuss basic energy saving techniques, such as identifying environment as in-vehicle, indoor, etc., to lower the battery usage by temporarily disabling PSM transmissions.

In addition to the proposed and implemented applications in previous and ongoing work, P2X transmissions from VRU devices such as smartphones create opportunities for enhancing safety and convenience. Consider, for example, the following applications, some of which are adapted from prior work:

VRUNearby. A version of this is arguable the most frequently considered safety application for P2X. It can inform drivers when potentially unexpected vulnerable road users are nearby. The application can function with approximately block-level positioning accuracy.

TFLAssistant. Traffic light assistant application can potentially improve cycle scheduling of the traffic lights, which maintains vehicle traffic flows and reduces pedestrian wait times.

WaitingForBus. A smart bus stop could estimate the number of people currently waiting and relay this information to arriving buses as well as collect it for transit planning purposes. This application needs position precision good enough to determine that a person is waiting near a bus stop.

VRUInStreet. This application notifies vehicles of VRUs that are currently located in the street rather than on the sidewalk. It is a more precise version of the *VRUNearby* application for urban areas based on the heuristic that a pedestrian who is walking on the sidewalk is safer than a pedestrian who is crossing a road. Readers are referred to [71] for more detail.

The examples above illustrate that requirements for position accuracy could potentially vary significantly across the application space. Although we later provide a set of preliminary positioning accuracy and minimum/maximum message rate requirements for the above applications for the purpose of simulation, determining the exact behavior of each application in detail is beyond the scope of this chapter.

6.2 Design Scope and Challenges

The frequent transmission of Pedestrian Safety Messages (PSMs) [13] that the aforementioned P2X applications require, could saturate the available channel capacity, particularly when other traffic shares the channel, and requires mitigation strategies that minimize energy consumption. In this chapter, we explore solutions to these issues.

First, in terms of channel congestion, Rostami et al. showed [60] that in crowded pedestrian scenarios such congestion can occur and degrade communication performance unless it is mitigated by congestion control. This can also affect the communication performance of other wireless traffic that may share the channel with PSMs in the future. In prior work, Tahmasbi et al. [73] introduced a context-aware congestion mitigation technique which leverages the content of BSMs received from vehicles to determine transmission power and message rate for sending pedestrian information. Rostami et al. [71] classified pedestrians as either *AtRisk* or *Safe* based on their estimated locations. PSMs of those deemed *Safe* may be suppressed to avoid channel congestion. While this research helps mitigate PSM-induced channel load, it does not prevent channel congestion when PSMs are mixed with other wireless traffic.

We therefore seek to approach the challenge through a context-aware transmission framework which controls channel congestion independent of message type on the channel for dynamic and different application requirements. We can fortunately leverage experience from V2V communication congestion control studies. For example, LIMERIC, standardized in [38], controls the channel load to a desirable range with no presumption on the type of messages. However, these V2V congestion control solutions, with LIMERIC included, require continuous measurement of the channel status and would cause unacceptable energy consumption for smartphones. For example, work by Zhang and Shin [74] showed that most of the energy consumption in wireless networks is due to Receive mode (RX) and Idle Listening mode (IL) at the physical layer. This observation raises questions whether smartphones can support channel congestion control.

Further, it remains hard to provide pedestrian devices with position information accurate enough to enable all P2X applications across a broad set of environments.

Jain et al. [47] shows that smartphone positioning accuracy in areas with clear sky view can support applications with high accuracy requirements like *VRUInStreet*. In urban canyons, however, tens of meters of error can occur and we are not aware of a technology to support such applications based only on smartphone sensors.

These observations indicate a time-varying demand for sending PSMs as a smartphone is carried around, a characteristic that potentially causes a more dynamic channel load and disturbs resource allocation of a congestion control algorithm. These existing congestion control algorithms have not been designed for a diversity of message rates across nodes that occur in heterogeneous application environment, such as where the applications' activities are controlled with context-aware transmission policies.

6.3 Heterogeneous Application Environment

6.3.1 System Architecture

Fig. 6.1 shows the proposed system architecture to support controlling of PSM-induced channel congestion. It includes two major components: a contextual PSM generation module and a Multi-Rate Controller. The first component manages the content of a PSM based on the aggregate requirements of P2X applications. The proposed system adopts a communication requirement manager that analyzes each application's requirement on the interval of sending a certain data element of PSM. Consolidation of these analyses yields a PSM with content to serve the needs of all applications. Meanwhile, a minimum and a maximum message rate to send the consolidated PSM are calculated and passed down to the multi-rate controller which will compute an appropriate PSM generation time according to the channel utilization status. This time is fed back to the communication requirement manager that controls the timing of the execution of the PSM generation sub-system. More details on the PSM generation time and the design of multi-rate controller can be found in Section 6.4.

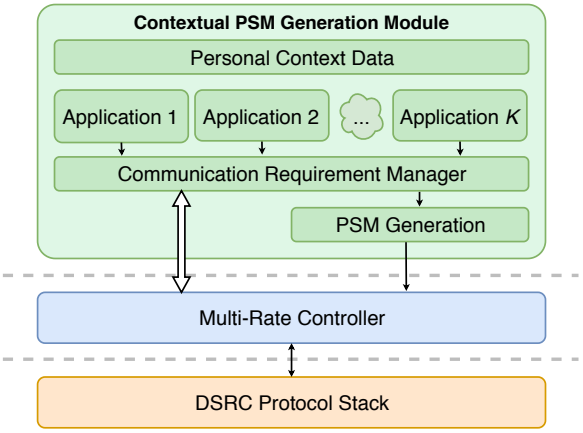

Figure 6.1: Contextual Transmission Policy Framework.

6.3.2 Contextual PSM Generation

The above system architecture preserves the flexibility of P2X application developers in defining how often and what elements of a PSM they want to transmit. From the example applications we surveyed, it appears such requirements vary across applications. Therefore, a set of requirements, e.g. minimum and maximum message rates, is assumed to be provided by the application developers in advance. For example, a pedestrian in a *WaitingForBus* application may not send PSMs as often as the one for walking across a street. This observation led us to leverage pedestrian context to manage the generation of PSM.

As an example, work in [43] showed a technique for detecting the moment of a pedestrian stepping down from the curb to the street. This technique could be used in future P2X applications to activate certain applications (that increase message rate) upon detection of such vulnerable moments. Another context clue that could be leveraged across applications in our survey for controlling PSM generation is the positioning system's current accuracy. Since most applications need a certain positioning accuracy to function as expected, we implement here a basic mechanism that pauses an application if its required positioning accuracy cannot be met.

6.4 Multi-Rate Controller

The design of our Multi-Rate Congestion Control algorithm is driven by the characteristics of PSM traffic. As mentioned in Section 6.3.2, a pedestrian may roam through several P2X use case scenarios with different PSM transmission requirements. Such time-varying demand in transmission of PSM is captured by the fluctuation of the minimum and maximum PSM transmission rate parameters in the communication requirement manager in Fig. 6.1. Therefore, the first two design questions for our multi-rate controller are: (i) how to allocate wireless channel resources for supporting multiple VRU devices that have different message rate requirements, and, (ii) how to adapt to the temporal change of PSM transmission rate requirement on an individual VRU device. Moreover, given the limited battery power a smartphone has, energy efficiency is a universal requirement in our design.

6.4.1 Proportional Fairness

The concept of proportional fairness for wireless resource allocation has been explored in the V2V congestion control context. We select multi-rate LIMERIC [70] as our starting solution. It allocates wireless resources in a proportionally fair manner to users with different application requirements as a result of message rate requirement aggregation. An example of rate aggregation strategy is explained in Section 6.3.2.

The question then becomes how to map various PSM transmission rate requirements to (α,β). To facilitate discussion, we use r^i_{min} and r^i_{max} to represent the aggregated minimum and maximum PSM rates by the communication requirement manager (see Fig. 6.1) of the i^{th} pedestrian user, respectively. In a general scenario, two users i and j may use different r_{min} and r_{max}. This leaves us a decision to make—how to represent the bandwidth requirement of the two users in a proportionally fair manner as a function of r^i_{min}, r^i_{max}, r^j_{min} and r^j_{max}. Let us first consider the case where sufficient channel bandwidth is available so that no user drops below the minimum rate and revisit the more general case in the following subsection.

We define r_{sys} as the system-defined maximum message rate allowed across the

entire system. All other chosen message rates across different users at different times must be less or equal to r_{sys}. Then, we choose to use the ratio of the two maximum PSM frequencies as the ratio of allocating wireless resource to the two pedestrian users, i.e. r^i_{max}/r^j_{max}. The rationale is that under ideal channel conditions (i.e., no channel congestion), the two users would transmit PSMs with a ratio of r^i_{max}/r^j_{max}. We aim to maintain this ratio as two pedestrian users reduce PSM rates due to channel congestion. It is shown in [70] that proportional message rates for different users is achievable through using similar α's and different β's, as congestion control parameters. Eq. 6.1 shows the relation between r and β.

$$\frac{\beta^i}{\beta^j} = \frac{r^i}{r^j} \tag{6.1}$$

6.4.2 Excessive Number of Users

Another design question arises when the available bandwidth cannot satisfy the minimum transmission requirement for all users. This may occur for PSM transmissions when large numbers of pedestrians cluster in a small area or when other data traffic shares the same channel.

Two prevailing methodologies which were derived in supporting V2V Basic Safety Message (BSM) communications may be applicable to our design. ETSI ITS-G5 prioritizes the calculated message rate by channel congestion control over the message rate required by individual vehicles. On the other hand, SAE J2945/1 [75] does the opposite and sets a minimum BSM transmission rate for BSMs and prioritizes it over the calculated rate by channel congestion control. While both seem to have a viable rationale, in our design, considering the wide spectrum of P2X applications, we use r^i_{min} as the lower bound interval of generating PSM for the i^{th} pedestrian user.

6.4.3 Time-Varying PSM Transmission Demand

An important design parameter for the proposed multi-rate controller is the algorithm convergence speed. A pedestrian potentially faces time-varying minimum and maximum message rates, i.e. (r_{min}, r_{max}), computed by the communication requirement

manger because of time-varying positioning accuracy or other context clues such as location. When a new (r_{min}, r_{max}) is provided for the same user, the legacy weighted-rate LIMERIC [70] takes a few seconds to converge to a new PSM rate corresponding to the newly provided pair and prevailing channel condition. Therefore, a complementary proactive mechanism to converge more quickly to the final PSM rate, i.e. r_{PSM}, seems necessary. This is particularly important for safety applications when they request a large increase from the previous r_{max}.

As mentioned before, the communication requirement manager module in Fig. 6.1 could potentially indicate different (r_{min}, r_{max}) at different times for an individual VRU device. Let $(r_{min}(t), r_{max}(t))$ be the minimum and maximum required message rates at time t. The PSM rate fairness, described in section 6.4.1, can be applied to the time-changing PSM rates as follows:

$$\frac{\beta^i(t)}{\beta^j(t)} = \frac{r^i(t)}{r^j(t)} \implies \frac{\beta^i(t_1)}{\beta^i(t_2)} = \frac{r^i(t_1)}{r^i(t_2)} \tag{6.2}$$

Therefore, the controller proactively calculates a system-wide PSM rate r_{cc}, corresponding to the r_{sys} by the upper layer. Using the available r_{cc}, the algorithm is able to calculate the PSM rate r_{PSM} corresponding to the provided (r_{min}, r_{max}) at time t using Eq. 6.3.

$$r_{PSM}(t) \leftarrow r_{cc}(t) \times (r_{max}(t)/r_{sys}) \tag{6.3}$$

Note that our proposed algorithm uses the characteristics described in Eq. 6.2 to directly calculate the final proportion of r_{cc}, i.e. r_{PSM}, without needing the specific β's.

6.4.4 Collaborative CBP Measurement

The key idea for energy-efficient design of the algorithm is that measuring CBP can be done by other devices rather than locally. We call these third-party nodes *Helpers*. The legacy LIMERIC algorithm from V2V uses measured CBP from the past intervals of $MonitorInv$ to adjust the message rate. Fig. 6.2 shows how the proposed collaborative CBP measurement mechanism breaks each $MonitorInv$ into a $CBPMeasInv$ during which *Helpers* measure CBP, and a $CBPSharinInv$, during which *Helpers* broadcast their measured CBP values using PSM. The key point is that regular smartphones, i.e.

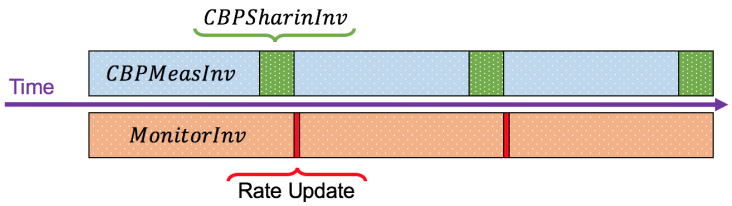

Figure 6.2: Illustration of different time intervals.

the consumers of broadcasted CBP values, do not need to listen to the wireless channel to measure CBP during $CBPMeasInv$. Instead, they can operate in TX-only mode during this time, and only switch to fully operational mode for the $CBPSharinInv$ to receive and calculate, CBP_{Rep}, i.e. the maximum reported CBP by nearby *Helper* nodes. There is a significant amount of work on synchronized sleep duties in the Wireless Sensor Networks (WSN) research area [76].

There are a few options to define *Helper* nodes. They could be devices which do not have energy limitations, i.e. they are not running on battery. Smart traffic lights or vehicles with radios operating on the same wireless channel are good examples. We call these approaches *RSUHelper* and *VehHelper*, respectively. If no infrastructure is available in the area, there is another option wherein during each CBP measurement and sharing cycle, some of the smartphones stay up for the entire period and spend more energy to measure CBP and further share the measured values with other smartphones at the end of the cycle. We call this approach *PedHelper*. In this work, we consider an approach where each smartphone draws a Bernoulli random variable at the beginning of each $MonitorInv$ and will play the *Helper* role with probability. Other more sophisticated selection procedures are also possible.

Algorithm 2 shows the steps that the proposed multi-rate controller takes to calculate r_{PSM}, i.e. the PSM rate. As the inputs of the algorithm, (r_{min}, r_{max}) is the pair of the aggregated minimum and maximum message rate by the upper layer, CBP_{Rep} is the maximum reported CBP by *Helpers* during the latest $MonitorInv$. First, the rate adjustment part of the algorithm uses closed-loop feedback to measure the difference between the desired CBP CBP_{target} and CBP_{Rep} (line 3). The resulting error CBP_{err} is further used to calculate the rate adjustment after checking for boundaries for one-step adjustment (lines 4-5). In the next step, the algorithm updates the system-wide

Algorithm 2 Multi-Rate Controller Algorithm

1: **Input:** (r_{min}, r_{max}), CBP_{Rep}
2: **Output:** r_{PSM}
3: $CBP_{err} \leftarrow CBP_{target} - CBP_{Rep}$
4: $CBP_{cap} \leftarrow \beta_{sys} \times CBP_{err}$
5: Boundary Check for CBP_{cap}
6: $r_{cc} \leftarrow (1 - \alpha) \times r_{cc} + CBP_{cap}$
7: $r_{PSM} \leftarrow r_{cc} \times (r_{max}/r_{sys})$
8: **if** $r_{PSM} > r_{max}$ **then**
9: $\quad r_{PSM} \leftarrow r_{max}$
10: **else if** $r_{PSM} < r_{min}$ **then**
11: $\quad r_{PSM} \leftarrow r_{min}$
12: **end if**

controller message rate r_{cc} (line 6) and then the PSM rate corresponding to the input pair of (r_{min}, r_{max}) is calculated using Eq. 6.3 (line 7). At the end, the new PSM rate is clipped to the allowed range (lines 8-12).

In summary, the following features are incorporated in the proposed congestion control module:

- The proposed algorithm can accept different pairs of (r_{min}, r_{max}) as input and provide fairness in terms of the final PSM rate offered to nodes using different sets.
- The proposed algorithm prioritizes r_{min} and r_{max}, requested by the Communication Requirement Manager (see Fig. 6.1), over its own calculated rate.
- The proposed algorithm proactively tracks a system-wide message rate and instantly calculates PSM rates for the requested pair of (r_{min}, r_{max}).
- The proposed congestion control algorithm does not rely on local CBP measurements.

6.5 Simulator Design

The proposed algorithms are evaluated via ns-3 simulations with a calibrated receiver model [28][27], a calibrated GPS model [72], and a calibrated channel model described in Chapter 2. As mentioned in Chapter 2, the channel model takes building shadowing factors into consideration.

6.5.1 Simulation Scenario

For the evaluation, the Times Square neighborhood in New York City is selected as the region of interest for the following reasons: 1) its pedestrian and vehicle density is particularly high; 2) it represents a challenging scenario for P2X communications due to aggregated interference from other transmitters; and, 3) it has been also identified as one of the priority intersections regarding pedestrian accidents. Manhattan overall accounts for 34 out of an average 157 annual New York City pedestrian fatalities [77].

The simulations use a publicly available mobility trace file for the Manhattan area (See Chapter 3). As mentioned before, the trace has been calibrated to account for an afternoon commute using pedestrian counts from personal observations and photos. To run simulations where RSUs are used as *Helpers*, the imported mobility trace is enriched with the coordination of traffic lights at each intersection.

Table 6.1: Simulation Configuration

Parameter	**Value**
CW_{min}	15
AIFSN	2
Packet size	316 bytes
Queue size	1 (oldest drop)
Transmission power	20 dBm
Noise floor	-98 dBm
Energy detection threshold	-85 dBm
Channel bandwidth	10 MHz
non-P2X Sharing Ratio	50%
$CBPMeasInv$	190 msec
$CBPSharinInv$	10 msec
$MonitorInv$	200 msec
CBP_{target}	79%
r_{sys}	10 Hz
β_{sys}	0.033
α	0.1

6.5.2 Simulation Configuration

Table 6.1 shows the default simulation parameters used in this section, which apply to all results unless noted otherwise.

For simulation purposes, P2X applications of Section 6.1 are considered. Table 6.2 shows the proposed applications and their required r_{max} and Minimum Positioning Accuracy (MPA) to stay functional. For simplicity, it is assumed that the required r_{min} for each application is $r_{min} = r_{max}/10$.

Table 6.2: Example P2X Applications

Application	r_{max}	**MPA**
VRUNearby	1 Hz	30 m
TFLAssistant	2 Hz	10 m
VRUInStreet	10 Hz	1 m
WaitingForBus	1 Hz	10 m

To the best of our knowledge, the DSRC channel hosting PSM communications, i.e. channel 176, is unlikely to be exclusively used for P2X communications. We therefore also consider scenarios where less bandwidth is available due to other traffic on the channel. These shared channel conditions are emulated via downgrading the data rate from the actual 6 Mbps (representing 0% sharing) to 3 Mbps to emulate 50% shared channel. One reason to avoid simulating extra non-P2X transmissions directly is that, to the date, it is unknown to us for what other purposes the channel could be used and what other devices will use the channel to transmit their data. Nevertheless, we do not expect a significant difference between the emulated simulation results with the case where extra transmission are simulated as well.

6.6 Results

In this section, the proposed algorithms are evaluated using the ns-3 simulator. We use Information Age (IA) as the primary evaluation metric for comparing the performance of our algorithms with the ones in prior work. The number of PSM transmissions, and the percentage of time spent in different PHY modes are the other evaluation metrics we used to analyze the simulation results. In the Baseline algorithm all the VRU devices transmit at a constant message rate of 10 Hz. Single-rate LIMERIC from the V2V literature is labeled as *V2V CC*, and the proposed algorithm, where smartphones play the Helper role is labeled as *PedHelper*.

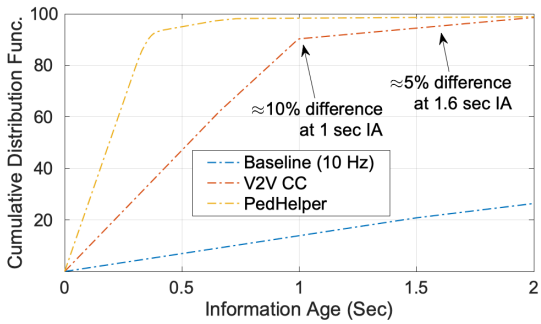

Figure 6.3: Information Age of a pedestrian with accurate positioning at nearby vehicles while crossing 7$^{\text{th}}$ Avenue.

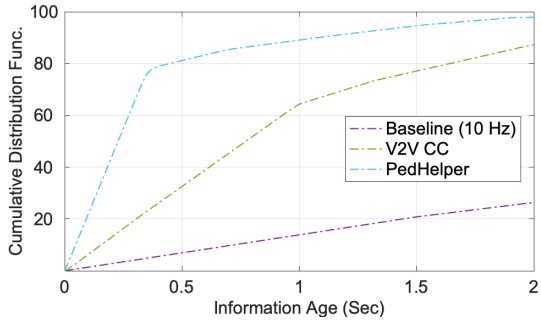

Figure 6.4: Information Age of a pedestrian with accurate positioning at nearby vehicles while crossing 7$^{\text{th}}$ Avenue using our proposed calibrated propagation model.

Fig. 6.3 shows the IA of a pedestrian crossing 7$^{\text{th}}$ Avenue. To eliminate randomness due to GPS positioning accuracy from the impact of different algorithms on IA, it is assumed that positioning accuracy of the subject's GPS sensor is sufficient to enable the *InStreet* application while crossing. The IA of the subject is calculated at nearby vehicles ($d < 150m$) while crossing. The Baseline algorithm suffers from a high packet error ratio, while *V2V CC* could not differentiate among contextual requirements, therefor all pedestrian devices converge to a similar low PSM rate. As a result, both algorithms show significantly worse IA in comparison with the proposed CTP framework.

To examine performance more accurately, similar simulations are run with the calibrated propagation model, presented in Chapter 2. Figure 6.4 shows the result using our calibrated intersection model. The baseline algorithm still suffers severe packet loss due to high packet collision. Although the performance of both V2V CC and PedHelper degraded after employing the new propagation model, it is clearly seen that our proposed algorithm still outperforms the V2V congestion control algorithm.

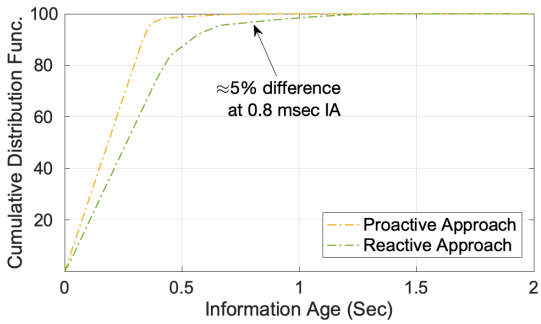

Figure 6.5: Information Age of a pedestrian with accurate positioning at nearby vehicles while crossing 7$^{\text{th}}$ Avenue using PedHelper algorithm with different PSM rate calculation approaches.

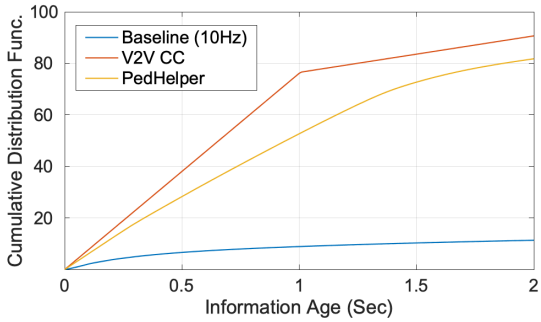

Figure 6.6: Information Age of pedestrians Operating at r_{max}=2 Hz around Times Square area.

As mentioned before, one of the enhancements of the proposed multi-rate controller in comparison with the legacy weighted-rate LIMERIC is the proactive message rate calculation. Gradually increasing the PSM rate when, for example, the pedestrian starts to cross the street would harm the safety application performance, i.e. *InStreet* application, because the VRU device transmits PSMs less frequently than the current channel load allows. Fig. 6.5 shows IA of a similar subject as in Fig. 6.3 for the first 3 seconds after stepping on the road. As illustrated, ≈5% of the cases have IA $>$ 800 msec which leads to longer detection times by the approaching vehicles and potentially increases accident risks.

One observation is that the non-safety applications, e.g. *TFLAssistant* and *WaitingForBus* in Table 6.2, would experience higher IA when *PedHelper* is employed. Fig. 6.6 shows IA for these applications. This happens primarily due to the proportional channel access by *PedHelper*. However, the IA is not a priority for such non-safety applications.

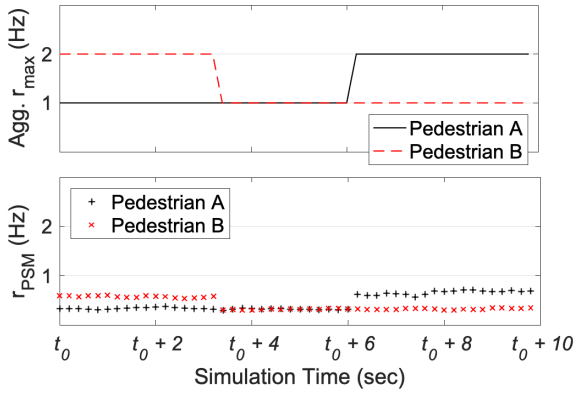

Figure 6.7: Calculated PSM rates by the proposed controller based on the input by the upper layer for two nearby pedestrians.

6.6.1 Proportional Fairness

As discussed in Section 6.4.1, the congestion controller should be able to maintain the ratio of the r_{max} rates provided by CTP. Fig. 6.7 shows the upper layer aggregated r_{max} rates (top), and the corresponding calculated PSM rates by the proposed algorithm (bottom) at two simulation nodes representing two pedestrians in a crowded scenario. These pedestrians are walking near each other and are , therefore, receiving similar CBP measurements from Helper nodes. This figure also shows the instant convergence of the algorithm when the upper layer indicates a new set of transmission requirements at time $t_0 + 3$ and $t_0 + 6$.

Fig. 6.7 illustrates the proportional fairness of r_{PSM} for two pedestrian devices with different (r_{min}, r_{max}), where the underlying controller keeps the same ratio when calculating the PSM rate, i.e. ≈0.66 Hz and ≈0.33 Hz, for $r_{max} = 2$ Hz and $r_{max} = 1$ Hz, respectively. The figure also illustrates how PSM rates change instantly.

What happens if no helper node is around or when the channel is underused? For a pedestrian walking in a less crowded area in the simulation scenario, the channel load is very low. CBP measurements are received less frequently as well, because less *Helpers* are around (or have been deployed in *RSUHelper*). Nevertheless, our proposed algorithm is able to cope with the situation and give the necessary freedom to smartphones to send PSMs more frequently while PSM rate does not exceed the r_{max} indicated by the upper layer.

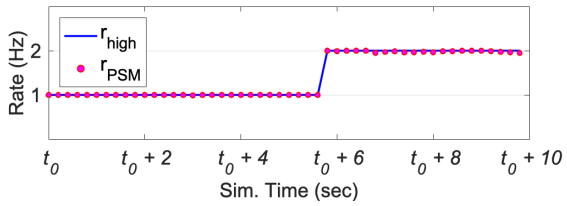

Figure 6.8: Aggregated maximum message rate and the calculated PSM rates by the multi-rate controller for a single pedestrian in a less crowded part of the map.

Fig. 6.8 illustrates a time-varying aggregated r_{max} by the upper layer and its corresponding calculated r_{PSM} through 10 seconds of simulation for a pedestrian walking in a less crowded area of the simulation map. It can be clearly seen that when possible, the proposed algorithm would not interfere with the system working at its maximum capacity.

6.6.2 Impact of Collaborative CBP Measurement

The primary advantage of the proposed collaborative CBP measurement mechanism is to let the radios to operate in TX-only mode for the majority of the time, and therefore, save a lot of the battery power. To evaluate the performance of our proposal, V2V LIMERIC, labeled as *V2V CC*, is compared to the proposed multi-rate controller in terms of energy consumption. Since the energy consumption for *RSUHelper* and *VehHelper* are similar, we omit the *VehHelper* results.

Note that since the exact amount of energy consumed by the radio is chipset-dependent, we compare the percentage of time that the radio spends in each modes during the simulation time. To provide one point of reference for interpretign the results, an Atheros AR5213 chipset documentation lists energy consumption for these modes as: TX = 127 mW, RX = 223.2 mW, IL = 219.6 mW, and SL = 10.8 mW [78].

Fig. 6.9 shows both a normalized overall energy consumption comparison and a detailed comparison using the normalized time spent in different PHY modes between the three aforementioned protocols. The top plot, shows that *V2V CC* consumes the most energy. The bottom plot shows the average percentage of time that the radios have spent in each PHY mode. Note that the bar marked with IL^* includes the total time listening to the idle channel, and identifying the channel as busy because

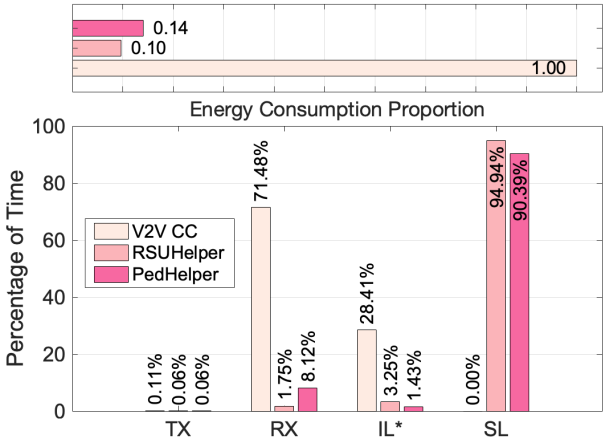

Figure 6.9: Energy consumption: Normalized total proportions (top), and detailed percentage of the time spent in each PHY modes (bottom)

the energy level on the channel is beyond the threshold. As the bottom plot shows, the reason for poor energy efficiency of *V2V CC* is that it spends more time in RX and IL^* modes because it requires the radio to continuously measure the CBP and piggybacking the measured CBP values on outgoing PSMs. Fig. 6.9 also shows that there is no significant difference between the *RSUHelper* and the *PedHelper* approaches, wherein the smartphones assume the role of Helper nodes.

The proposed collaborative CBP measurement, however, requires additional transmissions by Helpers. The additional burden is negligible as a very limited number of devices transmit these messages at relatively large intervals. Fig. 6.10 shows a channel busy percentage measured at the center of the busiest intersection in the simulation for PedHelper with and without the proposed collaborative CBP measurement mechanism. When locally measured, VRU devices operate in full capacity to measure CBP and piggyback the measured values over the PSMs. Therefore each VRU device has access to both locally measured CBP and its one-hop neighbors'. The observation is that the collaborative CBP measurement does not have a significant impact on the channel conditions in terms of channel busy percentage.

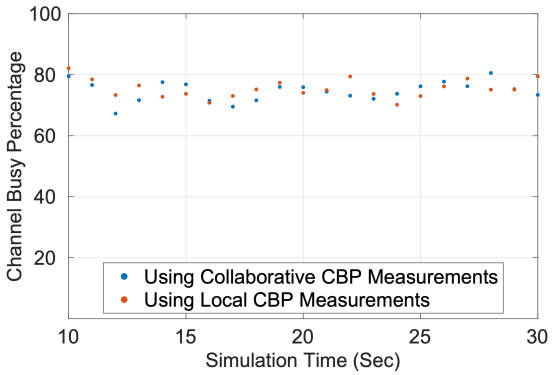

Figure 6.10: Channel busy percentage measurement for PedHelper algorithm with different CBP measurement mechanisms.

6.7 Conclusion

This chapter introduces an adaptive multi-rate congestion control algorithm to maintain channel load at desired levels, while allowing VRU devices to operate at different message rates in a heterogeneous application environment. It also lowers device energy consumption through a synchronized collaborative CBP measurement technique that allows smartphones' radios to spend more time in sleep mode. To evaluate the proposed multi-rate controller, a Contextual Transmission Policy (CTP) as an example source of a time-varying application requirement is also introduced. Simulation results with a Manhattan pedestrian simulation model show that this approach reduces channel congestion in busy urban canyon environments and improves information age for when safety applications are activated. It also shows that the proposed multi-rate congestion control algorithm with the proposed collaborative channel measurement mechanism reduces smartphone power consumption by 90% compared to legacy congestion control algorithms.

6.8 Chapter Summary

The contributions of this chapter are as follows:

- Designing an energy-efficient multi-rate congestion control algorithm that can operate in a dynamic and heterogeneous application environment to avoid channel

saturation in crowded areas or when background traffic is high.

- Introducing a cooperative channel load measurement mechanism to reduce battery consumption by liberating the radio from continuous monitoring of the channel for measuring channel load.
- Devising an example Contextual Transmission Policy to eliminate smartphone P2X message transmissions that provide little benefit to applications.

Chapter 7

Conclusions

7.1 Summary

In conclusion, this thesis studied pedestrian safety communication at scale through accurate simulation and introduced a multi-rate channel controller for heterogeneous pedestrian-to-everything communication applications. Overall, this dissertation has made the following contributions:

- We reported our large-scale data collection with 10 DSRC transceivers in a reference intersection. We used channel 172 to exchange Basic Safety Message (BSM) between the radios. We further analyzed the collected data, resulted in a scalable hybrid propagation loss model that is both geometrical in terms of using building geometry to distinguish between LOS and NLOS, as well as stochastic because the impact of buildings on propagation behavior is captured implicitly by a stochastic model. We showed that building structures have significant impact on propagation. We also find that existing intersection models do not fit the experimental data well, and that the proposed model shows considerable improvement over models by previous studies.

- We created a simulation scenario for Times Square area in New York City and generate pedestrian and vehicle traces using the Simulation of Urban Mobility (SUMO) simulator. Using these mobility traces, we evaluated channel load and performance of such a network. The evaluation is done considering sample transmission trigger policies that prioritize pedestrians based on their context where the transmission rate varies between 1 Hz and 5 Hz. Simulation results raise questions on whether vulnerable road user performance targets can be met in crowded

environments.

- We argued that the safety of Vulnerable Road Users (VRU), in particularly pedestrians, depends on their location more than their speed. We designed a Contextual Transmission Policy (CTP) to account for this, focused on risk classification of pedestrians that are walking outdoors. To give priority to pedestrians in the street, the CTP identifies potential in-street pedestrians with a classifier that checks for proximity to common crossing points and can also incorporate additional crossing detection heuristics. Pedestrians that are potentially in the street maintain a higher message rate while those determined to be relatively safe off-street use reduced message rates. Simulation results show an improvement in information age while channel load still remains high.

- We introduced an adaptive multi-rate congestion control algorithm to maintain channel load at a desired level, while allowing Personal Information Devices (PID) to operate at different message rates in a heterogeneous application environment. It also lowers device energy consumption through a synchronized collaborative CBP measurement technique that allows smartphones' radios to spend more time in sleep mode. To evaluate the proposed multi-rate controller, an example source of a time-varying application requirement is also introduced. Simulation results show that this approach reduces channel congestion in busy urban canyon environments and improves information age for when safety applications are activated. It also shows that the proposed multi-rate congestion control algorithm with the proposed collaborative channel measurement mechanism reduces smartphone power consumption compared to congestion control algorithms designed for vehicle-to-vehicle communication environment.

7.2 End Note

The popularity of smartphones presents the opportunity for utilizing them to collaborate with road entities. It has been already shown that smartphones can frequently communicate with vehicles and road infrastructure for safety and convenience purposes

via Personal Safety Messages (PSM). For example, vehicles can use this information to alert drivers or to automatically avoid or reduce the severity of a possible crash. This thesis shows that such a system needs more attention when deployed at a large scale because high interference in crowded areas can result in significant performance degradation. We resolve the channel congestion problem by proposing a multi-rate congestion controller. By considering the Age of Information at receivers as the key evaluation metric, this thesis' proposed congestion controller shows significant improvements. We envision that pedestrian-to-everything (P2X) communication can be used in a variety of environments to improve pedestrian safety as well as providing more convenience.

Bibliography

[1] National Highway Traffic Safety Administration (NHTSA). Traffic safety facts 2015 FARS/GES annual report. `https://crashstats.nhtsa.dot.gov/Api/Public/ViewPublication/812384`, 2017. [Online; accessed Jun-2017].

[2] National Highway Traffic Safety Administration (NHTSA). Traffic safety facts 2014 FARS/GES annual report. `https://crashstats.nhtsa.dot.gov/Api/Public/ViewPublication/812261`, 2016. [Online; accessed Jun-2017].

[3] Nathinal Highway Traffic Safety Administration (NHTSA). Traffic safety facts. `https://crashstats.nhtsa.dot.gov/Api/Public/Publication/812451`, 2017. [Online; accessed September-2018].

[4] World Health Organization. Who global status report on road safety 2013: supporting a decade of action. 2013.

[5] Tarak Gandhi and Mohan Manubhai Trivedi. Pedestrian protection systems: Issues, survey, and challenges. *Intelligent Transportation Systems, IEEE Transactions on*, 8(3):413–430, 2007.

[6] Tianyu Wang, Giuseppe Cardone, Antonio Corradi, Lorenzo Torresani, and Andrew T Campbell. Walksafe: a pedestrian safety app for mobile phone users who walk and talk while crossing roads. In *Proceedings of the Twelfth Workshop on Mobile Computing Systems & Applications*, page 5. ACM, 2012.

[7] Abdullah Al Masud, Md Nazrul Islam Mondal, and Kazi M Ahmed. Vehicular communication system for vehicle safety using RFID. In *Communications (MICC), 2009 IEEE 9th Malaysia International Conference on*, pages 697–702. IEEE, 2009.

[8] United States Department of Transportation (USDOT). USDOT Connected Vehicles Pilot Deployment (CVPD). `https://www.its.dot.gov/pilots/`. [Online; accessed September-2019].

[9] New York City Department of Transportation (NYCDOT). Applications defined for NYCDOT Connected Vehicles Pilot Deployment (CVPD). `https://www.cvp.nyc/cv-safety-apps`, . [Online; accessed September-2019].

[10] Amin Tahmasbi-Sarvestani, Hadi Kazemi, Yaser P Fallah, Mohammad Naserian, and Allan Lewis. System architecture for cooperative vehicle-pedestrian safety applications using dsrc communication. Technical report, SAE Technical Paper, 2015.

[11] John B Kenney, Gaurav Bansal, and Charles E Rohrs. LIMERIC: a linear message rate control algorithm for vehicular DSRC systems. In *Proceedings of the Eighth ACM international workshop on Vehicular inter-networking*, pages 21–30. ACM, 2011.

[12] Yaser P Fallah, ChingLing Huang, Raja Sengupta, and Hariharan Krishnan. Congestion control based on channel occupancy in vehicular broadcast networks. In *Vehicular Technology Conference Fall (VTC 2010-Fall), 2010 IEEE 72nd*, pages 1–5. IEEE, 2010.

[13] SAE J2945/9. Vulnerable Road User Safety Message Minimum Performance Requirements. March 2017.

[14] Javier Gozalvez, Miguel Sepulcre, and Ramon Bauza. Impact of the radio channel modelling on the performance of vanet communication protocols. *Telecommunication Systems*, 50(3):149–167, 2012.

[15] José Santa, Antonio F Gómez-Skarmeta, and Marc Sánchez-Artigas. Architecture and evaluation of a unified v2v and v2i communication system based on cellular networks. *Computer Communications*, 31(12):2850–2861, 2008.

[16] Johan Karedal, Fredrik Tufvesson, Taimoor Abbas, Oliver Klemp, Alexander Paier, Laura Bernadó, and Andreas F Molisch. Radio channel measurements at street intersections for vehicle-to-vehicle safety applications. In *2010 IEEE 71st Vehicular Technology Conference*, pages 1–5. IEEE, 2010.

[17] Kim Mahler, Panagiotis Paschalidis, Mike Wisotzki, Andreas Kortke, and Wilhelm Keusgen. Evaluation of vehicular communication performance at street intersections. In *2014 IEEE 80th Vehicular Technology Conference (VTC2014-Fall)*, pages 1–5. IEEE, 2014.

[18] Henrik Schumacher, Hugues Tchouankem, Jörg Nuckelt, Thomas Kürner, Tetiana Zinchenko, André Leschke, and Lars Wolf. Vehicle-to-vehicle ieee 802.11 p performance measurements at urban intersections. In *2012 IEEE International Conference on Communications (ICC)*, pages 7131–7135. IEEE, 2012.

[19] Thomas Mangel, Matthias Michl, Oliver Klemp, and Hannes Hartenstein. Real-world measurements of non-line-of-sight reception quality for 5.9 ghz ieee 802.11 p at intersections. In *International Workshop on Communication Technologies for Vehicles*, pages 189–202. Springer, 2011.

[20] Taimoor Abbas, Katrin Sjöberg, Johan Karedal, and Fredrik Tufvesson. A measurement based shadow fading model for vehicle-to-vehicle network simulations. *International Journal of Antennas and Propagation*, 2015, 2015.

[21] Ines Ugalde, Bin Cheng, Ali Rostami, Marco Gruteser, and Syed Amaar Ahmad. Repeatability of vehicular measurements on public roadways. In *Proceedings of the 11th Workshop on Wireless Network Testbeds, Experimental evaluation & CHaracterization*, pages 25–32. ACM, 2017.

[22] Christoph Sommer, David Eckhoff, Reinhard German, and Falko Dressler. A computationally inexpensive empirical model of ieee 802.11 p radio shadowing in urban environments. In *2011 Eighth International Conference on Wireless On-Demand Network Systems and Services*, pages 84–90. IEEE, 2011.

[23] Vehicles in Network Simulation (Veins). `https://veins.car2x.org/`.

[24] Thomas Mangel, Oliver Klemp, and Hannes Hartenstein. 5.9 ghz inter-vehicle communication at intersections: a validated non-line-of-sight path-loss and fading model. *EURASIP Journal on Wireless Communications and Networking*, 2011(1): 1–11, 2011.

[25] Mate Boban, Tiago TV Vinhoza, Michel Ferreira, Joao Barros, and Ozan K Tonguz. Impact of vehicles as obstacles in vehicular ad hoc networks. *IEEE journal on selected areas in communications*, 29(1):15–28, 2011.

[26] Network Simulator ns-3. `https://www.nsnam.org/`.

[27] Bin Cheng, Ali Rostami, and Marco Gruteser. Experience: accurate simulation of dense scenarios with hundreds of vehicular transmitters. In *Proceedings of the 22nd Annual International Conference on Mobile Computing and Networking (MobiCom)*, pages 271–279. ACM, 2016.

[28] Wireless Information Network Laboratory (WINLAB). V2V broadcast simulation patches for network simulator 3 (ns-3.16). `http://www.winlab.rutgers.edu/~gruteser/projects/patch/Frame-Capture.html`.

[29] Bin Cheng, Hongsheng Lu, Ali Rostami, Marco Gruteser, and John B Kenney. Impact of 5.9 ghz spectrum sharing on dsrc performance. In *2017 IEEE Vehicular Networking Conference (VNC)*, pages 215–222. IEEE, 2017.

[30] Mikio Yanagisawa, Elizabeth Swanson, and Wassim G Najm. Target crashes and safety benefits estimation methodology for pedestrian crash avoidance/mitigation systems. Technical report, 2014.

[31] SAE J2945/9. Performance Requirements for Safety Communications to Vulnerable Road Users. March 2016.

[32] New York City Department of Transportation (NYCDOT). Pedestrian Safety Action Plan for Manhattan. `http://www.nyc.gov/html/dot/downloads/pdf/ped-safety-action-plan-manhattan.pdf`, 2016. [Online; accessed September-2019].

[33] Michael Behrisch, Laura Bieker, Jakob Erdmann, and Daniel Krajzewicz. SUMO–Simulation of Urban MObility. In *The Third International Conference on Advances in System Simulation (SIMUL 2011), Barcelona, Spain*, 2011.

[34] Mobility traces and ns-3 code download page. `http://www.winlab.rutgers.edu/~gruteser/projects/pedsim/simdl.html`, 2016. [Online; accessed Dec-2019].

[35] Ali Rostami, Bin Cheng, Gaurav Bansal, Katrin Sjoberg, Marco Gruteser, and John B. Kenney. Stability Challenges and Enhancements for Vehicular Channel Congestion Control Approaches. *Intelligent Transportation Systems, IEEE Transactions on*, 17:2935–2948, April 2016.

[36] Kazushige Ouchi and Miwako Doi. Indoor-outdoor activity recognition by a smartphone. In *Proceedings of the 2012 ACM Conference on Ubiquitous Computing*, pages 600–601. ACM, 2012.

[37] Tessa Tielert, Daniel Jiang, Qi Chen, Luca Delgrossi, and Hannes Hartenstein. Design methodology and evaluation of rate adaptation based congestion control for vehicle safety communications. In *Vehicular Networking Conference (VNC), 2011 IEEE*, pages 116–123. IEEE, 2011.

[38] Gaurav Bansal, John B Kenney, and Charles E Rohrs. LIMERIC: A linear adaptive message rate algorithm for DSRC congestion control. *Vehicular Technology, IEEE Transactions on*, 62(9):4182–4197, 2013.

[39] Ching-Ling Huang, Yaser Pourmohammadi Fallah, Raja Sengupta, and Hariharan Krishnan. Intervehicle transmission rate control for cooperative active safety system. *IEEE Transactions on Intelligent Transportation Systems*, 12(3):645–658, 2011.

[40] Pengfei Zhou, Yuanqing Zheng, Zhenjiang Li, Mo Li, and Guobin Shen. Iodetector: a generic service for indoor outdoor detection. In *Proceedings of the 10th acm conference on embedded network sensor systems*, pages 113–126. ACM, 2012.

[41] Donnie H Kim, Younghun Kim, Deborah Estrin, and Mani B Srivastava. Sensloc: sensing everyday places and paths using less energy. In *Proceedings of the 8th ACM Conference on Embedded Networked Sensor Systems*, pages 43–56. ACM, 2010.

[42] Merryn J Mathie, Adelle CF Coster, Nigel H Lovell, and Branko G Celler. Accelerometry: providing an integrated, practical method for long-term, ambulatory monitoring of human movement. *Physiological measurement*, 25(2):R1, 2004.

[43] Shubham Jain, Carlo Borgiattino, Yanzhi Ren, Marco Gruteser, Yingying Chen, and Carla Fabiana Chiasserini. Lookup: Enabling pedestrian safety services via shoe sensing. In *Proceedings of the 13th Annual International Conference on Mobile Systems, Applications, and Services*, pages 257–271. ACM, 2015.

[44] Samuli Hemminki, Petteri Nurmi, and Sasu Tarkoma. Accelerometer-based transportation mode detection on smartphones. In *Proceedings of the 11th ACM Conference on Embedded Networked Sensor Systems*, page 13. ACM, 2013.

[45] Frame capture model patches for ns3, 2016. [Online; accessed jun-2017].

[46] Bin Cheng, Ali Rostami, Marco Gruteser, John B Kenney, Gaurav Bansal, and Katrin Sjoberg. Performance Evaluation of a Mixed Vehicular Network with CAM-DCC and LIMERIC Vehicles. In *Proceedings of Workshop of Smart Vehicles at IEEE WoWMoM*, pages 1–6. IEEE, 2015.

[47] Shubham Jain, Carlo Borgiattino, Yanzhi Ren, Marco Gruteser, and Yingying Chen. On the limits of positioning-based pedestrian risk awareness. In *Proceedings of the 2014 workshop on Mobile augmented reality and robotic technology-based systems*, pages 23–28. ACM, 2014.

[48] Massimo Bertozzi, Alberto Broggi, Mirko Felisa, Guido Vezzoni, and Michael Del Rose. Low-level pedestrian detection by means of visible and far Infra-Red tetra-vision. In *Intelligent Vehicles Symposium, 2006 IEEE*, pages 231–236. IEEE, 2006.

[49] Aaron Steinfeld, David Duggins, Jay Gowdy, John Kozar, Robert MacLachlan, Christoph Mertz, Arne Suppe, Charles Thorpe, and Chieh-Chih Wang. Development of the side component of the transit integrated collision warning system. In *IEEE Intelligent Transportation Systems Conference. Washington, DC*, 2004.

[50] Chika Sugimoto, Yasuhisa Nakamura, and Takuya Hashimoto. Prototype of pedestrian-to-vehicle communication system for the prevention of pedestrian accidents using both 3G wireless and WLAN communication. In *Wireless Pervasive Computing, 2008. ISWPC 2008. 3rd International Symposium on*, pages 764–767. IEEE, 2008.

[51] Mehrdad Bagheri, Matti Siekkinen, and Jukka K Nurminen. Cellular-based vehicle to pedestrian (V2P) adaptive communication for collision avoidance. In *Connected Vehicles and Expo (ICCVE), 2014 International Conference on*, pages 450–456. IEEE, 2014.

[52] IEEE Standard for Information technology– Local and metropolitan area networks– Specific requirements– Part 11: Wireless LAN Medium Access Control (MAC) and Physical Layer (PHY) Specifications Amendment 6: Wireless Access in Vehicular Environments, July 2010.

[53] Klaus David and Alexander Flach. Car-2-x and pedestrian safety. *Vehicular Technology Magazine, IEEE*, 5(1):70–76, 2010.

[54] Xinzhou Wu, Sundar Subramanian, Ratul Guha, Robert G White, Junyi Li, Kevin W Lu, Anthony Bucceri, and Tao Zhang. Vehicular communications using DSRC: challenges, enhancements, and evolution. *Selected Areas in Communications, IEEE Journal on*, 31(9):399–408, 2013.

[55] Xinzhou Wu, Radovan Miucic, Sichao Yang, Samir Al-Stouhi, James Misener, Sue Bai, and Wai-hoi Chan. Cars talk to phones: A dsrc based vehicle-pedestrian safety system. In *Vehicular Technology Conference (VTC Fall), 2014 IEEE 80th*, pages 1–7. IEEE, 2014.

[56] José Javier Anaya, Pierre Merdrignac, Oyunchimeg Shagdar, Fawzi Nashashibi, and Jose Eugenio Naranjo. Vehicle to pedestrian communications for protection of vulnerable road users. In *Intelligent Vehicles Symposium Proceedings, 2014 IEEE*, pages 1037–1042. IEEE, 2014.

[57] How Snapdragon and Honda are working to save lives with smartphones. `https://www.qualcomm.com/news/onq/2015/06/16/how-snapdragon-and-honda-are-working-save-lives-smartphones`. [Online; accessed Jun-2017].

[58] Laying the Foundation for Vehicle-to-Pedestrian Communications. `https://www.volpe.dot.gov/news/laying-foundation-vehicle-pedestrian-communications`.

[59] Tampa Connected Vehicle Pilot. `https://www.tampacvpilot.com/stay-informed/media-resources/`.

[60] Ali Rostami, Bin Cheng, Hongsheng Lu, John B Kenney, and Marco Gruteser. Performance and channel load evaluation for contextual pedestrian-to-vehicle transmissions. In *Proceedings of the First ACM International Workshop on Smart, Autonomous, and Connected Vehicular Systems and Services*, pages 22–29. ACM, 2016.

[61] T. Datta, S. Jain, and M. Gruteser. Towards city-scale smartphone sensing of potentially unsafe pedestrian movements. In *2014 IEEE 11th International Conference on Mobile Ad Hoc and Sensor Systems*, pages 663–667, Oct 2014.

[62] Maozhi Tang, Cam-Tu Nguyen, Xiaoliang Wang, and Sanglu Lu. An efficient walking safety service for distracted mobile users. In *Mobile Ad Hoc and Sensor Systems (MASS), 2016 IEEE 13th International Conference on*, pages 84–91. IEEE, 2016.

[63] Armir Bujari, Bogdan Licar, and Claudio E Palazzi. Movement pattern recognition through smartphone's accelerometer. In *Consumer communications and networking conference (CCNC), 2012 IEEE*, pages 502–506. IEEE, 2012.

[64] Android API. Location services. `https://developer.android.com/reference/android/location/Location.html`. [Online; accessed May-2017].

[65] OpenStreetMap. `https://www.openstreetmap.org/`. [Online; accessed Jul-2017].

[66] Sanjit Kaul, Marco Gruteser, Vinuth Rai, and John Kenney. Minimizing age of information in vehicular networks. In *Sensor, Mesh and Ad Hoc Communications and Networks (SECON), 2011 8th Annual IEEE Communications Society Conference on*, pages 350–358. IEEE, 2011.

[67] GPS horizontal position accuracy. `http://www.leb.esalq.usp.br/disciplinas/Molin/leb447/Arquivos/GNSS/ArtigoAcuraciaGPSsemAutor.pdf`. [Online; accessed Jun-2017].

[68] A Bourdeau, M Sahmoudi, and JY Tourneret. Tight integration of gnss and a 3d city model for robust positioning in urban canyons. In *ION GNSS*, 2012.

[69] Rudy Ercek, Philippe De Doncker, and Francis Grenez. Nlos-multipath effects on pseudo-range estimation in urban canyons for gnss applications. In *Antennas and Propagation, 2006. EuCAP 2006. First European Conference on*, pages 1–6. IEEE, 2006.

[70] Gaurav Bansal and John B Kenney. Achieving weighted-fairnessin message rate-based congestion control for dsrc systems. In *Wireless Vehicular Communications (WiVeC), 2013 IEEE 5th International Symposium on*, pages 1–5. IEEE, 2013.

[71] Ali Rostami, Bin Cheng, Hongsheng Lu, Marco Gruteser, and John B Kenney. Reducing unnecessary pedestrian-to-vehicle transmissions using a contextual policy. In *Proceedings of the 2nd ACM International Workshop on Smart, Autonomous, and Connected Vehicular Systems and Services*, pages 3–10. ACM, 2017.

[72] Ali Rostami, Bin Cheng, Hongsheng Lu, John B. Kenney, and Marco Gruteser. A light-weight smartphone gps error model for simulation. In *Workshop of Network-assisted Collaborative Automated Driving*. IEEE, In Press.

[73] Amin Tahmasbi-Sarvestani, Hossein Nourkhiz Mahjoub, Yaser P. Fallah, Ehsan Moradi-Pari, and Oubada Abuchaar. Implementation and evaluation of a cooperative vehicle-to- pedestrian safety application. *To be appeared on IEEE transportation systems magazine.*

[74] Xinyu Zhang and Kang G Shin. E-mili: energy-minimizing idle listening in wireless networks. *IEEE Transactions on Mobile Computing*, 11(9):1441–1454, 2012.

[75] Society of Automotive Engineers (SAE) International. On-Board System Requirements for V2V Safety Communications. SAE J2945/1, March 2016.

[76] Wei Ye, John Heidemann, and Deborah Estrin. Medium access control with coordinated adaptive sleeping for wireless sensor networks. *IEEE/ACM Transactions on Networking (ToN)*, 12(3):493–506, 2004.

[77] New York City Department of Transportation (NYCDOT). Pedestrian safety action plan for Manhattan. `http://www.nyc.gov/html/dot/downloads/pdf/ped-safety-action-plan-manhattan.pdf`, . [Online; accessed September-2019].

[78] Power Consumption. Energy efficiency comparisons of wlan products. *White paper, Atheros Comm*, 2004.